Lead Halide Perovskite and Nobel Metal Nanocomposites: Synthesis and Property

NEHA BAJAJ
(MS16013)

A dissertation submitted for the partial fulfilment of
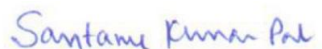
BS-MS dual degree in Science

Indian Institute of Science Education and Research Mohali

April 2021

Certificate of Examination

This is to certify that the dissertation titled "**Lead Halide Perovskite and Plasmonic Metal Nanocomposite: Synthesis and Property**" submitted by **Ms. Neha Bajaj** (**Reg. No. MS16013**) for the partial fulfilment of BS-MS dual degree programme of the Institute, has been examined by the thesis committee duly appointed by the Institute. The committee finds the work done by the candidate satisfactory and recommends that the report be accepted.

Dr. Santanu Kumar Pal
(Local/Administrative guide)

Dr. Angshuman Roy Choudhury
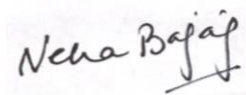
Dr. Subhabrata Maiti

Dr. Debrina Jana
(Supervisor)

Dated: April 30, 2021

Declaration

The work presented in this dissertation has been carried out by me under the guidance of Dr. Debrina Jana at the Indian Institute of Science Education and Research Mohali. This work has not been submitted in part or in full for a degree, a diploma, or a fellowship to any other university or Institute. Whenever contributions of others are involved, every effort is made to indicate this clearly, with due acknowledgement of collaborative research and discussions. This thesis is a bonafide record of original work done by me, and all sources listed within have been detailed in the bibliography.

Neha Bajaj

(Candidate)

Dated: April 30, 2021

In my capacity as the supervisor of the candidate's project work, I certify that the above statements by the candidate are true to the best of my knowledge.

Dr. Debrina Jana

(Supervisor)

Acknowledgement

It was a magnificent and inspiring journey to complete the BS-MS dual degree program at IISER Mohali. I want to express my gratitude to several people who assisted me in different ways during this course.

I want to express my sincere gratitude and graceful acknowledgement to my supervisor Dr. Debrina Jana for their guidance and valuable support throughout this work.

I gratefully acknowledge INSPIRE faculty research grant of Dr. Debrina Jana and, Notional allocation fund of IISER Mohali for funding this work. I am thankful to IISER Mohali central research facility for doing the TEM, SEM, Department of Science and Technology, India for providing INSPIRE scholarship throughout my academic program.

I would like to express thanks to my local guide Dr. Santanu Kumar Pal, project committee members Dr. Angshuman Roy Chaudhary and Dr. Subhabarta Maiti for their time and valuable suggestions that improved me to think more scientifically and understand the basic phenomena.

I acknowledge the Department of Chemical Sciences for providing a departmental teaching laboratory and other experimental and computational facilities. IISER Mohali for other central facilities, Library, and computer centre for their continuous support, stores and purchase section for their timely efforts. I also thank the office of the dean of academics for maintaining our academic records and making our study period smooth, the office of dean students for maintenance of our hostel and mess and the office of the registrar and accounts for our fellowship and other financial as well as administrative matters.

I express my gratitude to Mr. Akhilesh Meena, who worked along with me in the completion of this thesis work.

I am grateful to my lab members Ms. Saumya Sebastian and Mr. Deepraj Verma, for being supportive lab members. My sincere thanks to Mr. Yogendra Nailwal, Mr. Madhusudan Maiti, Mr. Mayank Joshi, Dr. Mrinal Kanti Adak and Ms. Labhini Singla, for their continuous encouragement and support. I also thank my friends in IISER Reena Yadav,

Satvik Singh, Prerna Goel, Rahul Singh Yadav, Umakant Gaurav, and Yuvraj Vaishnav for all the fun and boosting my confidence during these difficult COVID times.

Finally, yet importantly, I express my sincere gratitude to my beloved parents for their blessings and my siblings for their help and wishes for the successful proceedings of this project work.

<div align="right">Neha Bajaj</div>

List of Figures

List of Tables

Notations and Abbreviations

Au   Gold

Au@SiO$_2$@CsPbBr$_3$ Gold nanorods shelled with silica sphere which has CsPbBr$_3$ inside the mesoporous Silica.

CTAB   Hexadecyltrimethylammonium bromide

EDS   Energy Dispersive X-ray Spectroscopy

GNR   Gold Nanorods

LSPR   Localized Surface Plasmon Resonance

Pd   Palladium

Pd@ SiO$_2$@CsPbBr$_3$ Palladium nanorods shelled with silica sphere which has CsPbBr$_3$ inside the mesoporous Silica.

SEM   Scanning Electron Microscopy

SiO$_2$@CsPbBr$_3$ Silica spheres containing CsPbBr$_3$ inside them.

TCSPC   Time-Correlated Single Photon Counting

TEM   Transmission Electron Microscopy

Contents

Page No

Abstract

Perovskites have been on the headlines of current research due to the presence of exotic electrical and optical properties, phenomenal carrier transport characteristics, great photoluminescence quantum yield along with adjustable wavelength all across the visible spectrum, facile colour tunability, and improved stability.[1] The reported $CsPbBr_3$ perovskite is a well-known lead halide perovskite offering a great spectral range in the visible region.[2] In order to enhance its performance further, localized surface plasmon resonance (LSPR) produced by metallic nanoparticles can come handy. LSPR makes s use of metallic nanostructures to dramatically enhance the efficiency of radiative recombination in the active medium where electrons and hole combine.[3]

Conducting metals when placed nearby a fluorophore can either increase or decrease the electric field felt by the adjacent fluorophore, which can, in turn alter the decay rate.[4] The modification in the decay rate is likely to produce various applications in optoelectronic devices by increasing the photostability and quantum yield.

Herein, we prepared a nanocomposite of gold nanorod shelled by Silica with $CsPbBr_3$ inside the mesoporous Silica and compared its characteristics with mesoporous silica with $CsPbBr_3$ inside and Pd nanorods shelled with mesoporous Silica containing $CsPbBr_3$ inside it. Nanocomposite of $Au@SiO_2@CsPbBr_3$ can pave its way to usage in LEDs. The comparison of it with $SiO_2@CsPbBr_3$ will clearly illustrate the importance of plasmonic nanorod, and along with $Pd@SiO_2@CsPbBr_3.$ It will draw an insight on the effect of non-plasmonic material on this system in visible range, as outside visible range mainly in Ultraviolet and Infrared region Pd is plasmonic.

CHAPTER -1

Introduction

1.1 Nano-plasmonics

Nano-plasmonics is made up of two words: nano (in nanometer size range) and plasma. Plasma is a system where we have a whole bunch of positive and negative charges that are free to travel about without interfering with one another. It involves the use of tiny metallic particles, such as gold, silver, and copper spheres, to significantly improve the interaction between light and matter. These effects only take place if the particles are comparatively smaller than the wavelength of light. Since visible light has wavelengths measured in thousands of nanometers, particles must be smaller than 20 nm.
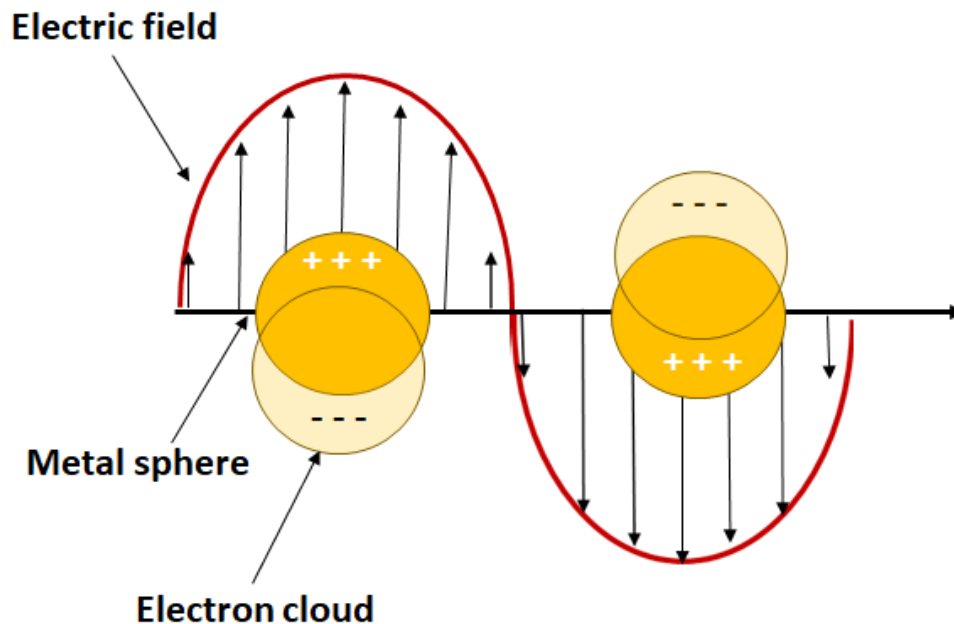
Figure 1: Surface Plasmon Resonance diagram showing oscillation of free conducting electrons due to strong interaction with incident light.(Redrawn from reference [5]).

1.2 Properties of Plasmonic Metals

As light illuminates plasmonic particles, they are primarily influenced by three properties.[6] These are as follows:

i. Electromagnetic Enhancement: Plasmons are excited in these nanoparticles when light is shone on them. These plasmons raise the electric field in a small region. These serve as nano-antennas or amplifiers, using the electric field of light to mirror it and generate their own electric field, but only in a specific area around them. The field produced in this small area is hundreds or sometimes even thousands of times more powerful than the incident light. Electromagnetic enhancement is a term for a boost in the intensity of the field in a small area.

ii. Resonant Frequency: All nanoparticles plasmonic responses do not handle all wavelengths equally. There is plasmonic resonance at a particular wavelength if the frequency of electric field enhancement is plotted against wavelength. The mountain is at its highest point here.

iii. Variation of Resonant Frequency: Since the resonant frequency is not a fundamental property, it is subject to change as the environment changes. It is largely determined by material, shape, size and environment around the nanoparticle.

In contrast to other nanomaterials, the properties of plasmonic materials stand out, enabling them to be used in a range of applications such as chemical and biosensors, photovoltaics, electronics, and optics.[7]
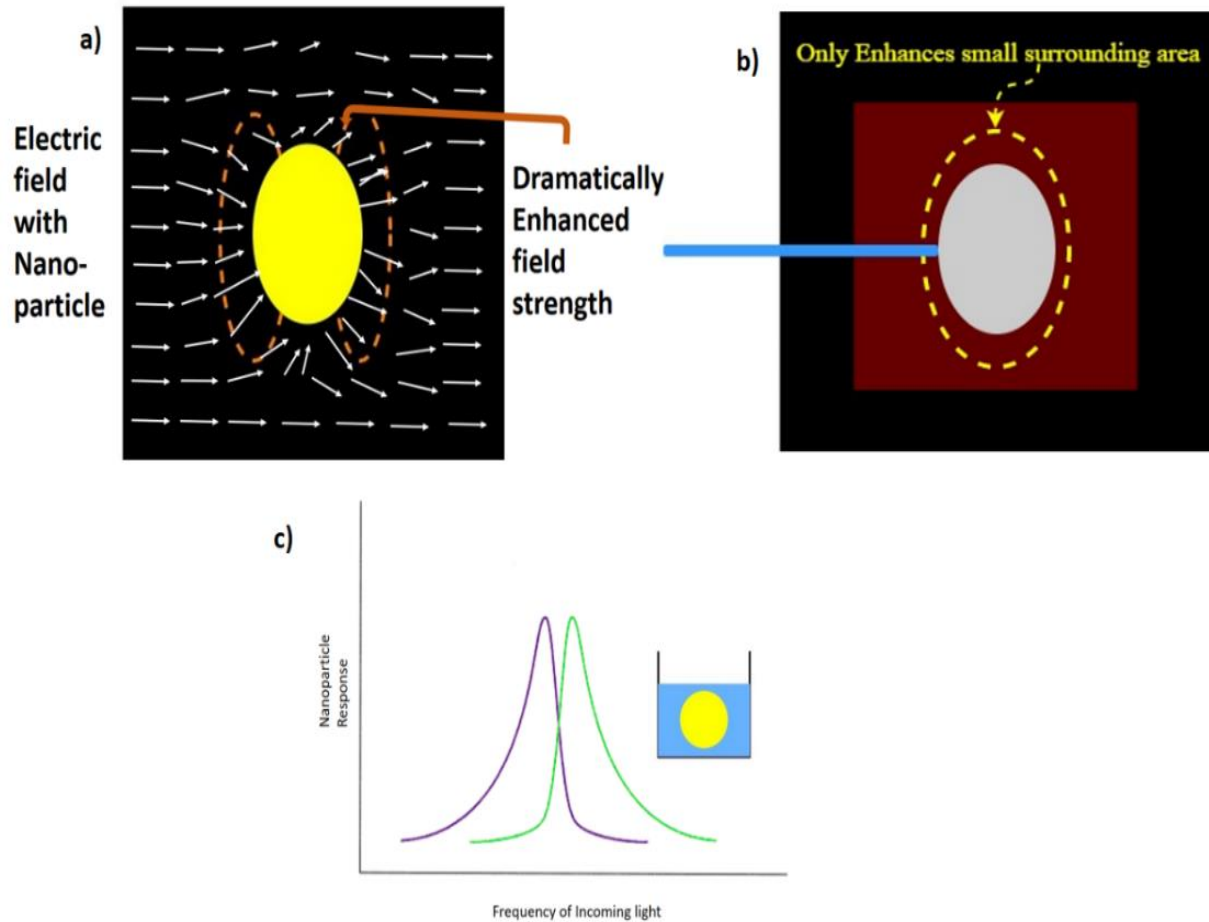
Figure 2: (a) Illustration of the effect of an electric field on a dipole moment (b) An illustration of how plasmons increase the electric field in a small area, and (c) Illustration of the effect of surrounding media on the resonant frequency.

1.3 Metal-Enhanced Fluorescence

In normal fluorescence, solutions are typically transparent to emitted radiations, and fluorophores emit into free space. Nearby conducting metallic particles will change the free-space conditions by increasing or decreasing the electric field felt by the fluorophore, thereby affecting the decay rate. The improvement in the radiative decay rate is referred to the rate at which fluorophore decays spontaneously. This process is also known as Metal-Enhanced

Fluorescence.[4]
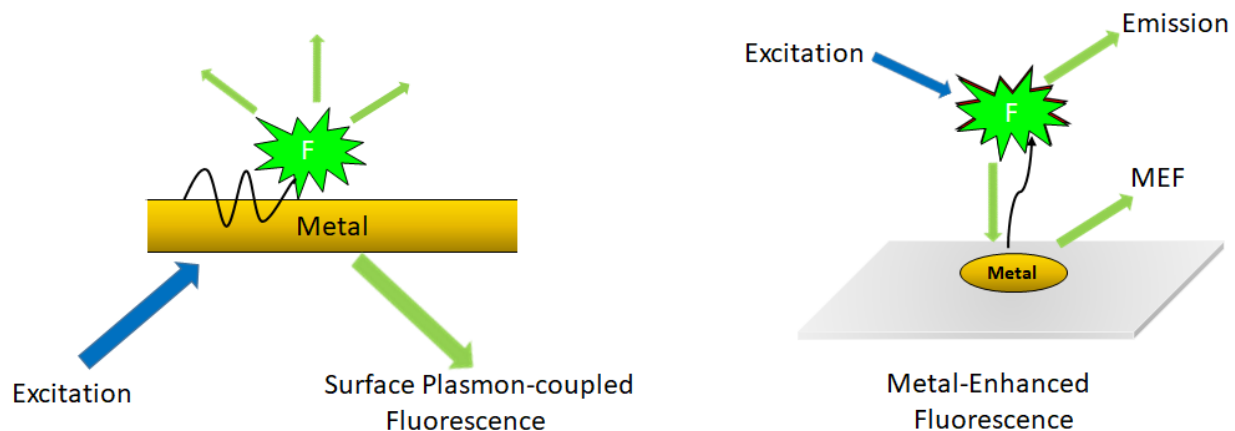
Figure 3. Schematic diagram depicting the impact of metal particles on fluorescence. (Redrawn from reference [4])

When metal is absent electrons are excited from ground state (S_0) to excited state (S_1) decay takes place radiatively and non-radiatively. However, with the presence of metal modifies the rate of radiative decay and thus extra decay rate is added which is termed as the modifies decay rate.

S_0 - Ground State
S_1 - Excited State
E – Excited State
E_m – Excitation Rate
Γ - Decay rate
Γ_m - Decay rate in presence of metals
K_{nr} - non radiative decay rate
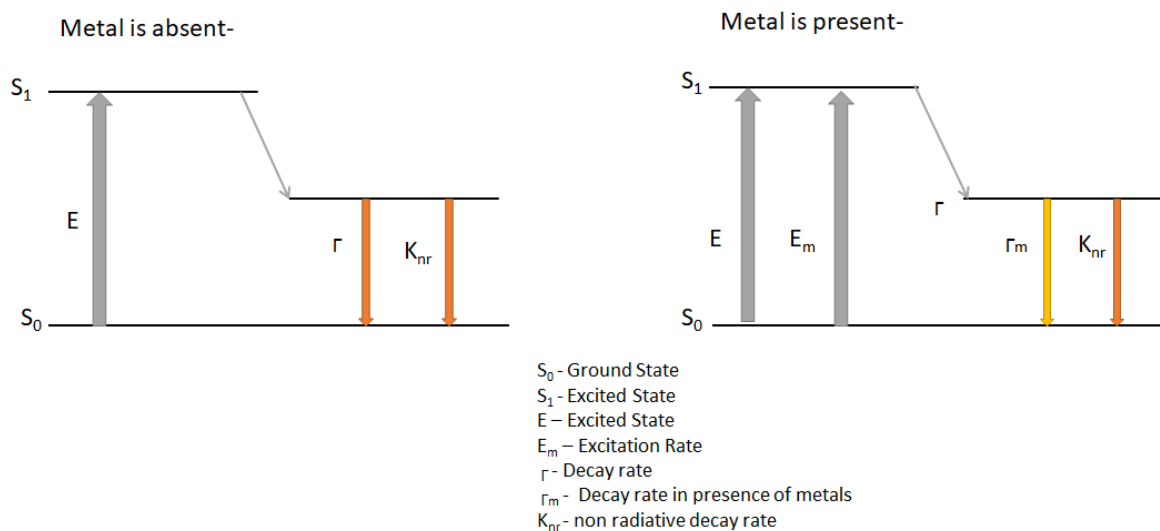
Figure 4: Jablonski diagram explaining the concept of Metal Enhanced Fluorescence. (Redrawn from reference [8])

1.4 Perovskites

Another distinctive class of materials are Perovskites. Perovskites are an intriguing class of nanomaterials with an ABX_3 crystal structure, in which A and B are cations, and X is an anion. Optoelectronics, energy production, superconductivity, and other applications are all possible with these nanomaterials. The corners of the cube occupy A cation, and the faces are occupied by small atom X with a negative charge. Large B cation is placed at the body centre of the cuboctahedral position. Cations occupy every hole that is created by BX_6 octahedrons.[9]

(a)

(b)
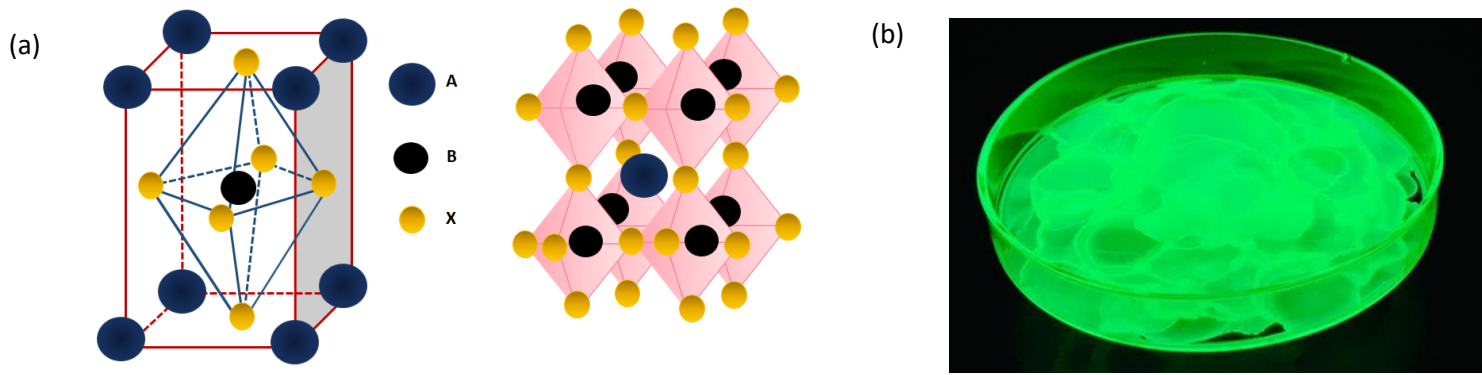
Figure 5: (a) Illustration of ABX_3 type perovskite structure.[9] (Redrawn from reference [9]) (b) $CsPbBr_3$ under UVlight (λ_{exc} 365nm).

Perovskites have a cubic structure, according to several reports. With the advancement of time, it was seen that some structures had large distortions from the symmetry of thought material. Thus, Goldschmidt came to the rescue and pointed out that perovskite is stable only if the parameter t (known as tolerance factor) is approximately near to unity. The tolerance factor represented by t is defined as follows:

$$t = \frac{r_A + r_X}{\sqrt{2}(r_B + r_X)}$$

Here r_a, r_b and r_x are denoted as the radii of ions. As a result, the Goldschmidt tolerance factor (t) or simply known as the tolerance factor, is an empirical index used for predicting the stability of a perovskite structure. Materials with t values ranging from 0.9 to 1 are considered ideally cubic, whereas those with t values ranging from 0.71 to 0.9 are considered distorted perovskites. If the t factor goes above 1 or less than 0.71, then it is regarded as a non-perovskite structure.[2]

Perovskites offer a high-spectral range in the visible region, are highly stable, provide large quantum yield, have high carrier mobility and provide great optical and electrical properties.

1.5 Properties of Perovskites

In addition to their tunable bandgaps, which also helps in tuning the color, low exciton binding energies, and long-range carrier diffusion, Perovskites have high optical absorption coefficients and narrow-band bright photoluminescence.[10] They also have a wide wavelength range in the visible region which makes them suitable for many practical applications. They also exhibit exotic electrical properties with great charge transport within the system.

Because of these properties, perovskites outperform conventional semiconductors such as silicon. Most notably, the easy synthesis of perovskites in the form of high-purity perovskites.

1.6 Use of Dielectric Media or Spacer

Metal nanoparticles are sensitive to moisture and oxygen. As a result, it is critical to shell these metal nanoparticles in order to provide chemical and thermal stability. This shelling also facilitates its use in a variety of applications. LSPR efficiency rises as the distance between the spacer and the metal nanoparticle decreases. However, if the distance is held too short, nonradiative quenching will occur, so it is essential to find a suitable distance for higher quantum efficiency and electroluminescence enhancement. Two main determining factors of the spacer are refractive index and coating thickness. The appropriate distance range typically ranges from 5 to 20 nm.[11,12]

1.7 Related Work:

Many researchers tried to bring fluorophores and plasmons together. Yang *et al.,* studied the effect of Au nanoparticles on $CsPbBr_3$ and tried using them in laser sources.[13] Zhang *et al.,* reported a 25 % increment in the luminescence of $CsPbBr_3$ using Au-Ag alloy nanoparticle.[14] Pan *et al.,* verified enhancement in electroluminescence by incorporating gold nanoparticles in a quantum dot light-emitting diode.[15] Xia *et al.,* studied the synergistic impact of Au nanorods and MgO on the PV (PhotoVoltaic) performance of $CH_3NH_3PbI_3$ based perovskite solar cells (PSCs).[16] Balakrishnan *et al.,* anchored Au nanoparticles on the surface of $CsPbBr_3$ and observed an increase in photocatalytic activity and applicability in light energy harvesting.[17] Zhang *et al.,* reported Ag-$CsPbBr_3$ system for plasmonic-perovskite LEDs.[18]

For LSP coupling to occur, it is required to match the LSP resonance and emission wavelength. Another critical factor in improving the coupling between emitters and metallic nanoparticles is the coupling distance. Moreover, these small metallic nanoparticles are sensitive to oxygen and moisture. Core/shell nanoparticles can help in solving this problem by facilitating chemical and thermal stability. Few studies have tried to explore this. Yun *et al.,* improved the luminescence of $CsPbBr_3$ by proposing stretchable plasmonic templates of Au and Au/SiO_2.[19] Dadi *et al.,* underlined the plasmonic enhancement of perovskite quantum dot films enabled by Au nanoparticles embedded into polymeric films.[20] Fan *et al.,* reported the synthesis of Au nanospheres or nanorods shelled with TiO_2 and used them to examine the plasmonic effect in planar perovskite solar cells.[21] Mali *et al.,* demonstrated improved photovoltaic performance of PSCs based on $Au@TiO_2$ nanofibres.[22] Wu *et al.,* illuminated the efficient enhancement of PSCs up to 17.6% by employing silica-coated gold nanorod.[23]

1.8 Current Work:

This study aims to determine how plasmonic nanocrystals affect the luminescent properties of perovskites. Our technique is to entrap gold nanorods in a silica matrix that has $CsPbBr_3$ encapsulated in it. In order to capture a snapshot of this, two other nanocomposites, $SiO_2@CsPbBr_3$ and $Pd@SiO_2@CsPbBr_3$ are also prepared to compare their characteristics. $SiO_2@CsPbBr_3$ has mesoporous Silica with $CsPbBr_3$ inside, and $Pd@SiO_2@CsPbBr_3$ has Pd nanorods shelled with mesoporous Silica containing $CsPbBr_3$ inside it. Nanocomposite of $Au@SiO_2@CsPbBr_3$ has the potential to pave its way to biosensing applications and usage in LEDs. The comparison of it with $SiO_2@CsPbBr_3$ will clearly illustrate the importance of plasmonic nanorod, and along with $Pd@SiO_2@CsPbBr_3$ will draw insight on the effect of non-plasmonic material on this system in the visible range as outside visible range Pd is plasmonic.

In order to explain the thought process behind this work, few questions need to be answered. These include the reasons to choose the materials in the formation of three-tier nanocomposite which has Au nanorod , silica matrix and $CsPbBr_3$.

The first is why gold is preferred over other plasmonic nanocrystals such as copper and silver. The following are the reasons:

- Gold is comparatively less reactive and more stable.[23]
- Its synthesis process is facile and can be replicated easily, resulting in the formation of It monodisperse particles.[24]
- It has a high level of conductivity.[23]
- It also posses strongly enhanced and tunable optical properties.[25]

Another question is the preference of gold nanorods in comparison to other shapes available like nanospheres or nanostars etc. It is well known that sharper the shape or more the number of edges higher is the SPR (Surface Plasmon Resonance). The reasons for its preference are as follows:

- They can be easily prepared.
- We can easily obtain monodisperse particles.
- We can have rational control over their aspect ratio.[26]
- One of the major points is that they show two types of plasmonic frequency – transverse and longitudinal frequency.[27]
- They also show long-range electromagnetic decay.[28]

Another query to be addressed is the need to shell Au with a silica matrix. A layer of silica matrix on top of SiO_2 provides various advantages. These include:

- High refractive index gives Mie resonance.[29]
- High chemical and mechanical stability along with good biocompatibility.[30]
- Facile surface functionalization.[31]
- Tunable pore size.[32]
- Providing an insulating surface layer and preventing light from scattering much.[33]
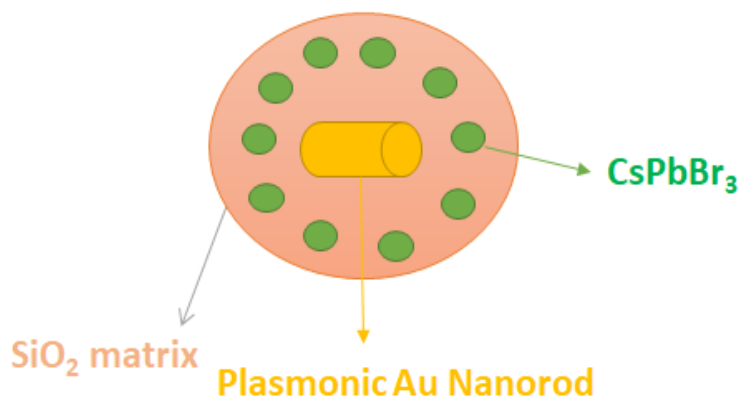
Figure 6: Schematic showing gold nanocomposite which has gold nanorods inside mesoporous silica with CsPbBr$_3$ encapsulated inside the pores of it.

1.9 Instrumentation

1.9.1   UV-Vis Spectroscopy

UV-Vis Spectra of the aqueous Au nanorod as well as of Au@SiO$_2$ and Au@SiO$_2$@CsPbBr$_3$ film were measured with the help of Cary 5000 UV-Vis NIR (Agilent Technologies) spectrophotometer at the scan rate of 1 nm/s. Cuvette made up of Quartz with path length 1 cm at room temperature was put into use for recording the spectra. Baseline correction with the corresponding solvent was done every time to eliminate the effect of solvent in the spectrum. In the case of glass slides, a clean glass slide was used as a baseline.

1.9.2 Transmission Electron Microscopy (TEM)

Transmission electron microscopy (TEM) studies were performed with the help of JEOL model JEM-F200, which is equipped with an Energy Dispersive X-ray Scattering facility (EDS). The sample preparation of TEM was done by drying a drop of suspension of particles in the corresponding solvent on a piece of carbon-coated Cu grid inside a hot air oven for some time and then keeping under vacuum conditions.

1.9.3 Field Emission Scanning Electron Microscopy (FESEM)

Field Emission Scanning Electron Microscopy (FESEM) was done using JEOL-7600F. The samples for FESEM were prepared using small pieces (8mm × 8mm) of Silicon wafers and drop-casting the solution prepared in the corresponding solvent evenly on the surface of the wafer. It was then dried by keeping it under vacuum.

1.9.4 Photoluminescence (PL) Spectroscopy

Photoluminescence Spectroscopy was done using HORIBA Fluoromax-4 with slit widths of 1 nm × 1 nm and a scan integration time of 1 s at an excitation wavelength λ_{exc} = 375 nm. The liquid samples were dispersed in the corresponding solvents, and in the case of glass slides, they were properly placed at an angle in the 10mm Quartz cuvette to obtain the PL spectra.

1.9.5 Time-Correlated Single Photon Counting (TCSPC)

Time-Correlated Single Photon Counting (TCSPC) was done with the help of Horiba Fluorohub-B using an excitation wavelength of 375 nm equipped with a picosecond diode laser at a repetition rate of 1 Mhz. The liquid samples were dispersed in the corresponding solvents, and in the case of glass slides, they were properly placed at an angle in the 10mm Quartz cuvette to obtain the TCSPC data. Neutral –Density Filter (ND Filter) was put into use when the alpha value (α) was going more than 2%.

1.9.6 Thermo Gravimetric Analysis (TGA)

TGA analysis was performed with the help of DTG-60H from Shimadzu, keeping the heating rate of 5 ⁰C per min up to 400 ⁰C.

CHAPTER 2

Synthesis and Characterization of Au nanocomposite (Au@SiO$_2$@CsPbBr$_3$)

2.1 Experimental Section

2.1.1 Chemicals Required

Hexadecyltrimethylammonium bromide (CTAB, C$_{19}$H$_{42}$BrN, ≥99.9%, Sigma-Aldrich), L-Ascorbic Acid (C$_6$H$_8$O$_6$, ≥99.7%, Sisco Research Laboratories), Silver Nitrate (AgNO$_3$, >99%, Sisco Research Laboratories), Sodium Borohydride (NaBH$_4$, ≥96%, Sigma-Aldrich), Gold(lll) chloride trihydrate (HAuCl$_4$.3H$_2$O, ≥49.0%, Sigma-Aldrich), Sodium Hydroxide pellets (NaOH, 98%, Sisco Research Laboratories), Methanol (CH$_3$OH, Avantor Performance Materials India Limited), Lead (II) Bromide (PbBr$_2$, 98%, Sigma Aldrich), Cesium Bromide (CsBr, 99.9%, Alfa Aeser), Ethanol (CH$_3$CH$_2$OH, Sigma Aldrich), N, N-Dimethylformamide (C$_3$H$_7$NO,99.8%, Sigma Aldrich), Hexane fraction from Petroleum (Merck Life Science Private Limited) and Milli-Q.

2.1.2 Synthesis of Au nanorods

182.2 mg of CTAB is added to 4.5 ml of Milli-Q and is mixed with 208 μl of 24 mM HAuCl$_4$.3H$_2$O. Subsequently, 100 μl of 100 mM Ascorbic acid is added, and the solution turns from dark yellow to colorless. Following this, 7.5 μl of 100 mM AgNO$_3$ and 50 μl of NaBH$_4$ is added with a minimal time interval. The prepared GNR (Gold Nanorod) solution is kept aside for few minutes until it turns purplish-black.
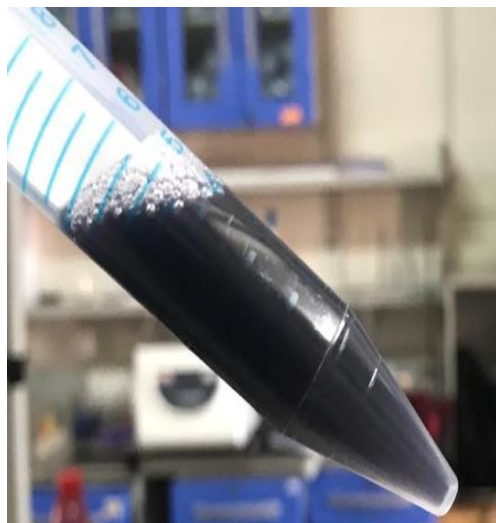
Figure 7: Digital picture showing the blackish-violet coloured solution of GNR in daylight.

2.1.3 Synthesis of Silica Shell over Au nanorods

The GNR solution is centrifuged for 30 min at 14000 rpm to remove excess CTAB and other impurities present. For this, the solution needs to be centrifuged to remove excess impurities as Ag^+ from $AgNO_3$ can bind with Br^- from CTAB and form a precipitate that needs to be removed.10 ml of Milli-Q is added to the pellet obtained, and UV-Visible spectrum is taken to know the exact absorbance, and Beer Lambert's Law ($A = \epsilon cl$) is applied to obtain concentration (c) where path length is 1 cm. Usually, the concentration obtained ranges from 0.40 to 0.65 nM. 20 mM solution of CTAB is prepared, and 1ml of it is loaded into the solution. The solution is aged overnight. The solution is then kept at continuous stirring by adding 15 μl of 0.1 M of NaOH. After 30 min, 20 μl of 50% TEOS in methanol is added. This addition is repeated twice after every 1 hr. The solution is then removed from stirring and kept for ageing for 24 hr. It is then washed with methanol for 30 min at 14000 rpm for 30 min to obtain a pellet.[36,37]

2.1.4 Variation in the thickness of the shell

Shell thickness can be varied by altering the concentration of TEOS, ageing time and stirring time.[38,39] Out of these three, varying the concentration of TEOS is the best method to increase the width of the shell. In the protocol described above, instead of using the 50% concentration of

12

TEOS every time, make three sets one by using 40%,50% and 60%, respectively. By varying the stirring time, it was observed that the shell was spilling and was losing its spherical morphology.

.

Figure 8: Solutions with varying TEOS concentration during the synthesis of silica shell on top of GNR.

2.1.5 Impregnation of CsPbBr$_3$ on Au@SiO$_2$

The pellet is dissolved in a minimal amount of methanol and is drop-casted on a clean glass slide (Washed with a soap-water solution and then given a quick boil in isopropanol). Then, 0.025 M PbBr$_2$ in N, N-Dimethylformamide is drop-casted and dried at 60 ˚C for 5 min. After that, 0.1 M CsBr in ethanol-water (9:1) is drop-casted and dried at a temperature around 60˚C for the duration of 2 min, and excess is wiped by Kim wipes. The slide is then kept under continuous vacuum for 1-2 hr. When it is completely dried, the powder is extracted and dissolved in hexane.

2.2 Results and Discussion

Synthesis of Au nanocomposite is a three-step process.[24] First step involves the formation of Au nanorods. Gold nanorods are prepared with the help of CTAB, HAuCl$_4$, Ascorbic acid, NaBH$_4$ and AgNO$_3$. Here, CTAB is the shape-directing surfactant; Ascorbic acid and NaBH$_4$ are the two reducing agents; HAuCl$_4$ is the gold source, and AgNO$_3$ is used to regulate the aspect ratio or growth of the nanorods. Two reducing agents of different reductive capabilities are required to

provide a time lag for the growth of nanorod, so is the reason that first, we need to add ascorbic acid, which is a weak reducing agent and then we need to add $NaBH_4$, which is a strong reducing agent to reduce Au^{+3} to Au^0.[34] This single pot methodology makes the procedure quite adaptable for replicating. The second step is to shell gold nanorods with the help of Silica. This acts as a dielectric media or spacer that provides an appropriate distance between the plasmonic nanoparticle and the fluorophore.[35] The third step is to insert $CsPbBr_3$ in a silica matrix. This is done by making ionic solutions as ionic solutions penetrate better inside the matrix in comparison to hot injection synthesized $CsPbBr_3$.

GNR   GNR@SiO$_2$ GNR@SiO$_2$@CsPbBr$_3$
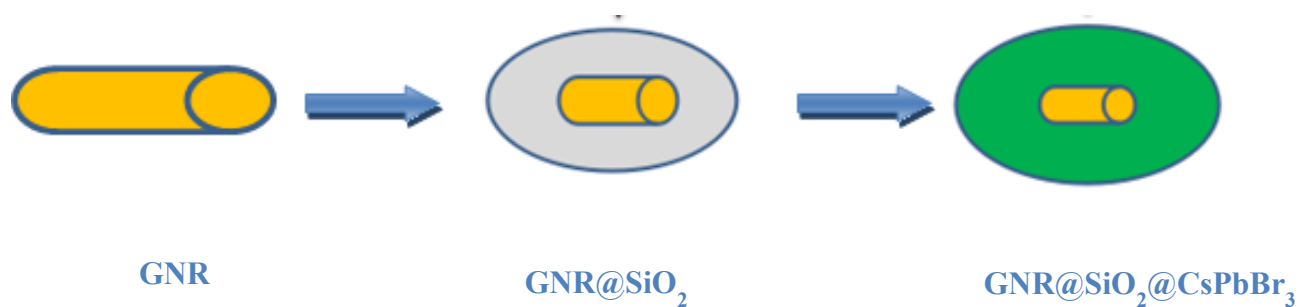
Figure 9: Schematic showing the three steps (formation of GNR, shelling with silica, insertion of $CsPbBr_3$ inside) to be followed in the given order for preparation of gold nanocomposite.

Various type of characterization techniques are required in order to confirm the formation of the proposed nanocomposites and also their analysis. We made use of UV-Visible Spectroscopy, Fluorescence Spectroscopy, Transmission Electron Microscopy (TEM), Scanning Electron Microscopy (SEM) and Time –correlated Single Photon Counting (TCSPC).

The formation of GNR is confirmed using UV-Visible spectroscopy as well as TEM images. It is evident from TEM images that there is the formation of a significant number of nanorods. UV-Visible spectrum depicts the two characteristic peaks of GNR where one is the transverse peak and another is the longitudinal peak. The transverse peak in this case is observed at 527 nm and the longitudinal peak is observed at 715 nm.
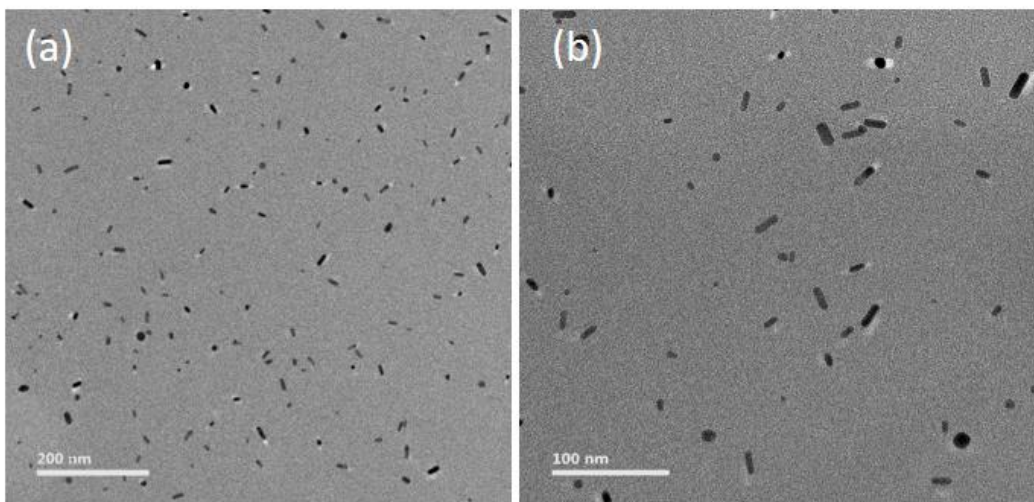
Figure 10: (a,b) TEM images showing the formation of monodisperse GNR.
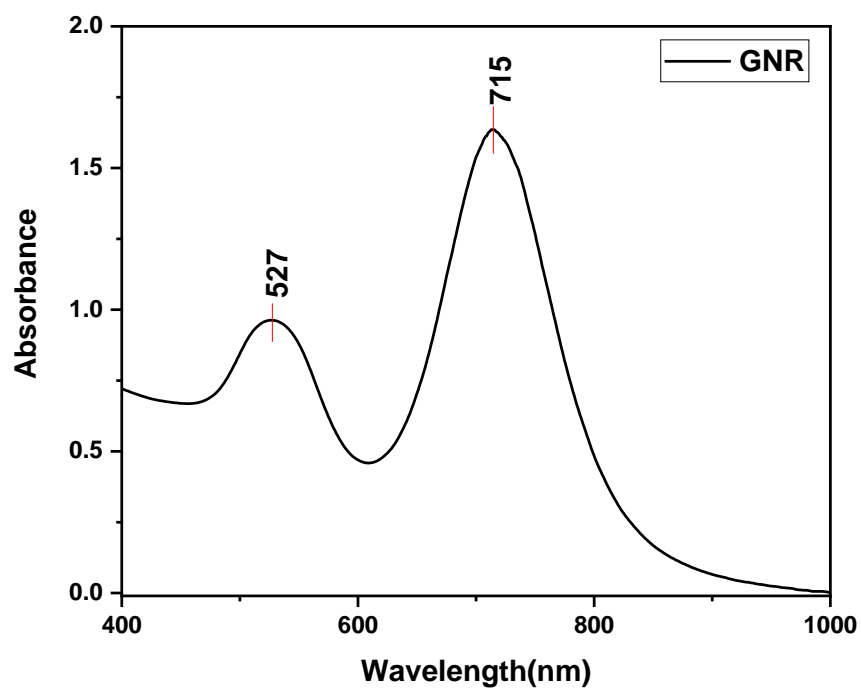
Figure 11: UV-Visible spectrum of GNR with its characteristic transverse and longitudnal plasmonic frequencies.

TEM images also confirm that each Au nanorod or GNR has been properly shelled with Silica spheres. The shell thickness is 6.26 nm which is pretty much in the range of appropriate distance (5-20 nm) for separation of Plasmonic metal and fluorophore. UV-Visible spectrum of GNR@SiO$_2$ (Au@SiO$_2$) shows a significant red shift in both the plasmonic frequencies, thus confirming the formation of a shell over Au nanorods.
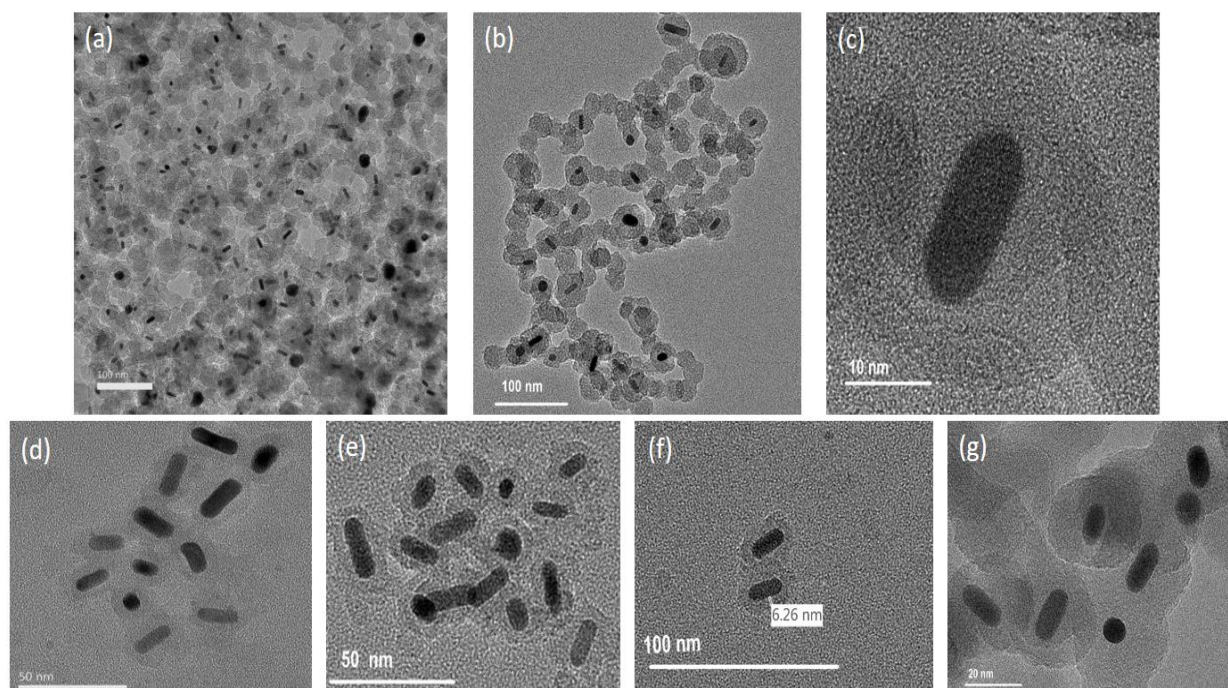
Figure 12: (a, b, c, d, e, f, g) TEM images of GNR@SiO$_2$.

The UV-Visible spectrum of Gold Nanorods (GNR) and Au@SiO$_2$, when plotted simultaneously, clearly shows a red shift when Au nanorods are shelled with Silica, thus also confirming its formation. The shift in the peaks could be due to varying refractive index of water and silica (GNR solution is prepared in Milli-Q).
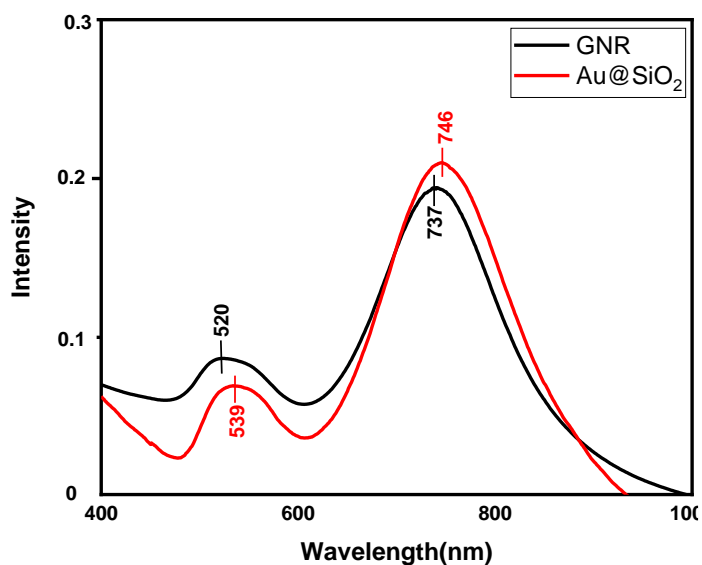
Figure 13: UV-Visible Plot of GNR and GNR@SiO$_2$ showing red shift after formation of silica shell on GNR.

The TEM-EDX analysis (Energy Dispersive X-ray Spectra using Transmission Electron Spectroscopy) gives an insight into the chemical composition of Au@SiO$_2$. Peaks corresponding to each constituent element is shown in the plot. The peak corresponding to non-constituent element C has been eliminated as it arises because of using the Carbon grid. The table below the graph gives information about the atomic % ratios present in Au@SiO$_2$@CsPbBr$_3$ obtained from TEM-EDX analysis.
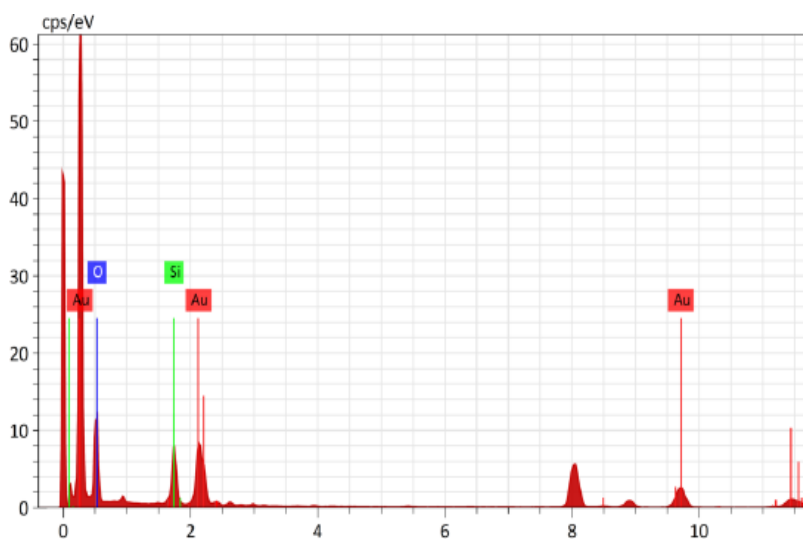
Figure 14: TEM-EDX analysis showing peaks of elements present in GNR@SiO$_2$.

Element	At. No.	Mass [%]	Atom [%]
Silicon	14	16.45	27.37
Oxygen	8	19.69	57.49
Gold	79	63.85	15.14
		100.00	100.00

Table 1: Atomic % ratio and mass % ratio of GNR@SiO$_2$.

Tomography by High Angle Annular Dark Field (HAADF) mode in TEM instrument provides a three-dimensional view of the internal structure of the Au@SiO$_2$ sample. It shows how Au nanorods are completely surfaced by the mesoporous silica shell.
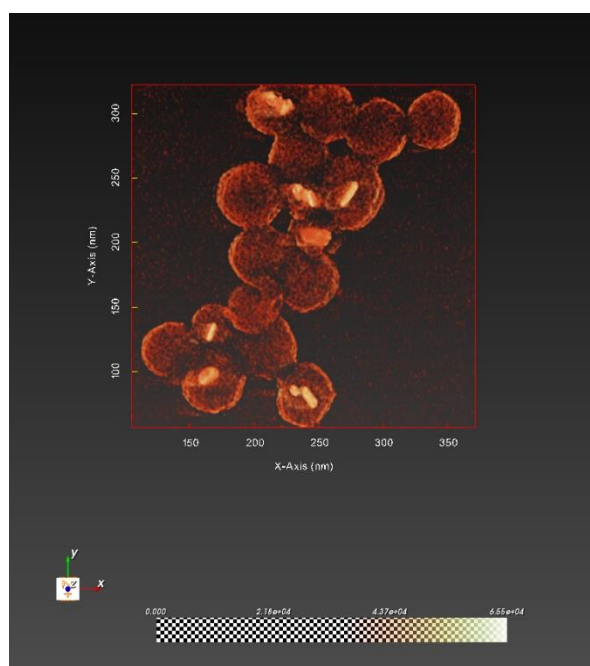
Figure 15: Tomography by HAADF mode in TEM of Au@SiO$_2$ sample.

The shell thickness can also be varied by changing the concentration of TEOS. Thus, as per the requirements, I played with the thickness of the silica shell by varying the concentration from 40% to 60 %.
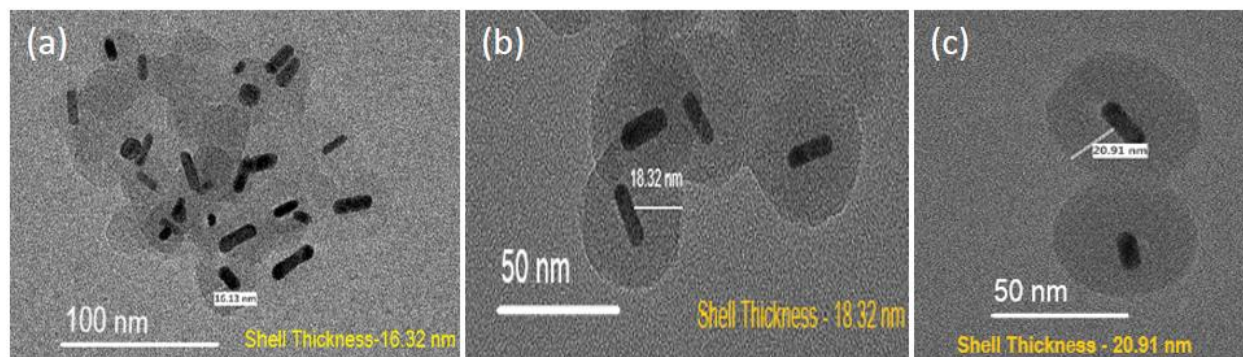
Figure 16: (a, b, c) Varying thickness of silica on GNR dispersed in methanol.
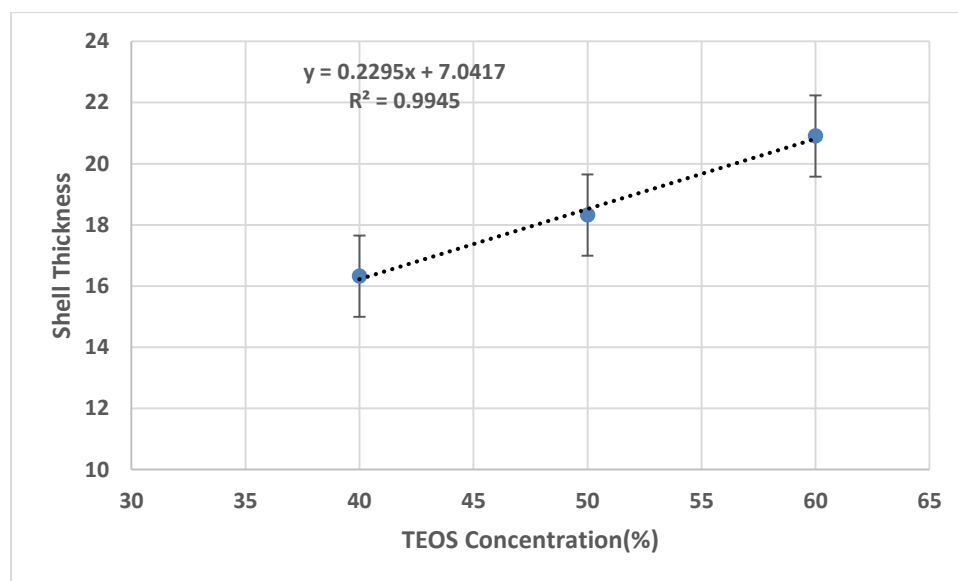
Figure 17: Plot of TEOS concentration vs Shell thickness.

There was also an impact of ageing time on the thickness of the shell. After the addition of TEOS, one solution was kept for ageing for 8 hr, and the other was kept for 96hr. There was a significant increment in the thickness of the silica shell after increasing the ageing time.
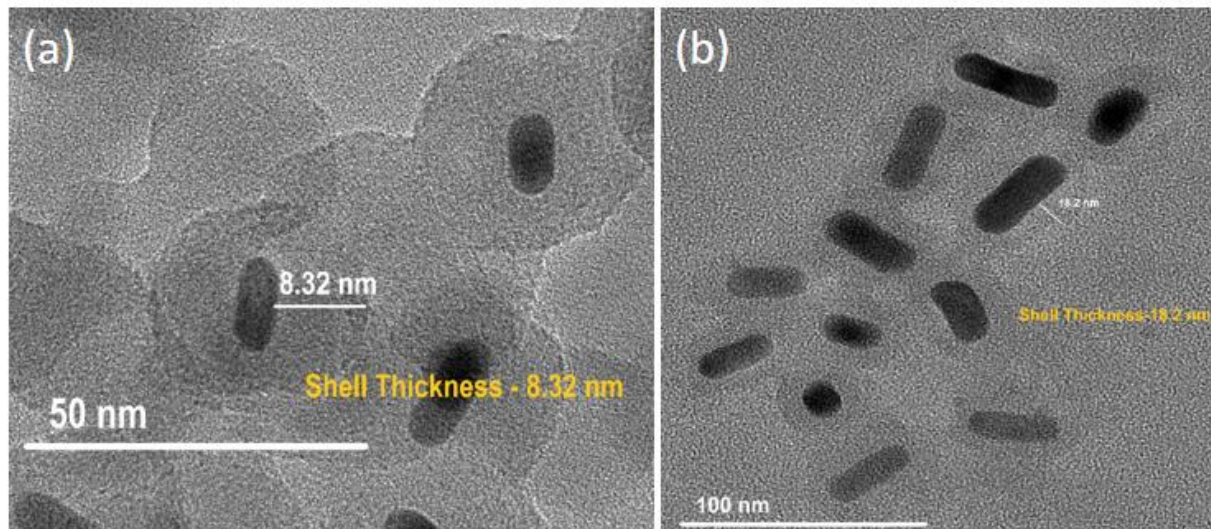
Figure 18: (a, b) Varying silica shell thickness on GNR due to different stirring time.

The image of the glass slide of Au@SiO$_2$@CsPbBr$_3$ taken under the excitation of 365nm confirms that CsPbBr$_3$ has gone into the mesoporous sphere of Silica and hence is showing luminescence. The PL plot of Au@SiO$_2$@CsPbBr$_3$ shows a peak at 510nm, which is the characteristic emission peak of CsPbBr$_3$. It also depicts the increment in the intensity of Au nanocomposite due to the presence of Au, a plasmonic material.
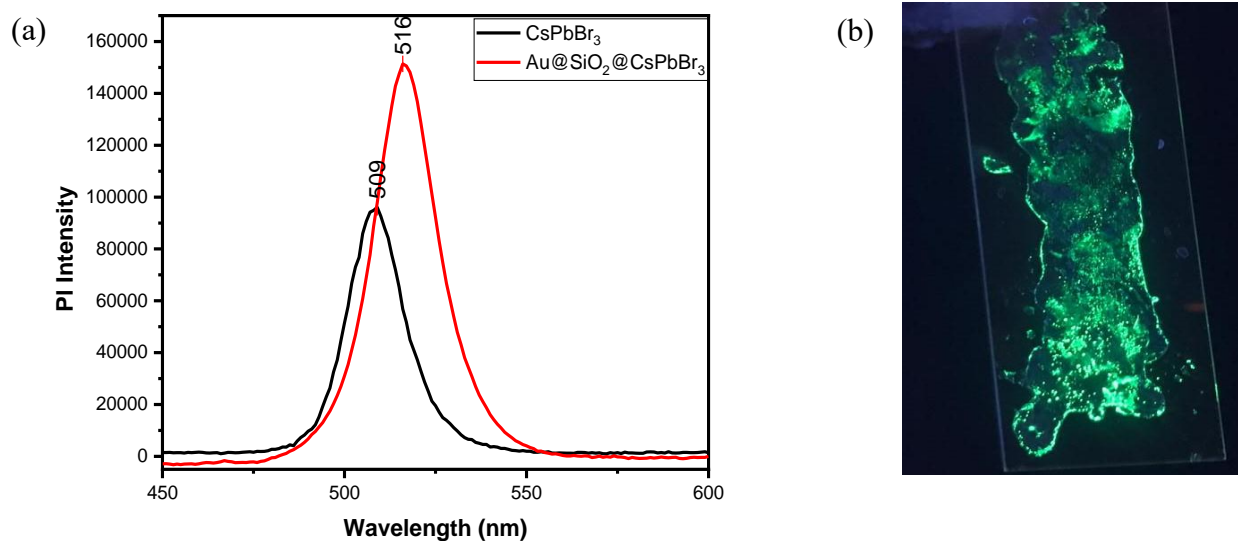
Figure 19: (a) PL spectra of $CsPbBr_3$ in comparison to $Au@SiO_2@CsPbBr_3$ (b) $Au@SiO_2@CsPbBr_3$ under UV light (λ_{exc} 365nm).

The lifetime analysis of $Au@SiO_2@CsPbBr_3$ was done with the help of Time Correlated Single Photon Counting.
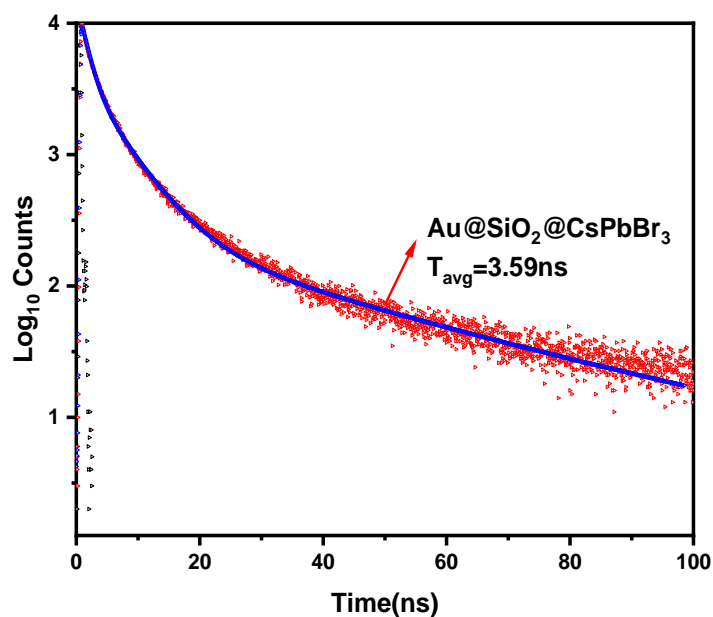
Figure 20: TCSPC Plot of $Au@SiO_2@CsPbBr_3$.

Sample	A_1	A_2	A_3	$T_1(ns)$	$T_2(ns)$	$T_3(ns)$	$T_{avg}(ns)$	χ^2
Au@SiO₂@CsPbBr₃	0.34	0.10	0.56	3.80	21.0	0.42	3.59	1.67

Table 2: Amplitude and corresponding lifetime of Au@SiO$_2$@CsPbBr$_3$.

Elemental color mapping with the help of Scanning Electron Microscopy also helped in confirming the elements present (mainly Au, Si, Cs, Pb and Br) in the nanocomposite and also depicts the variation of it over the surface.
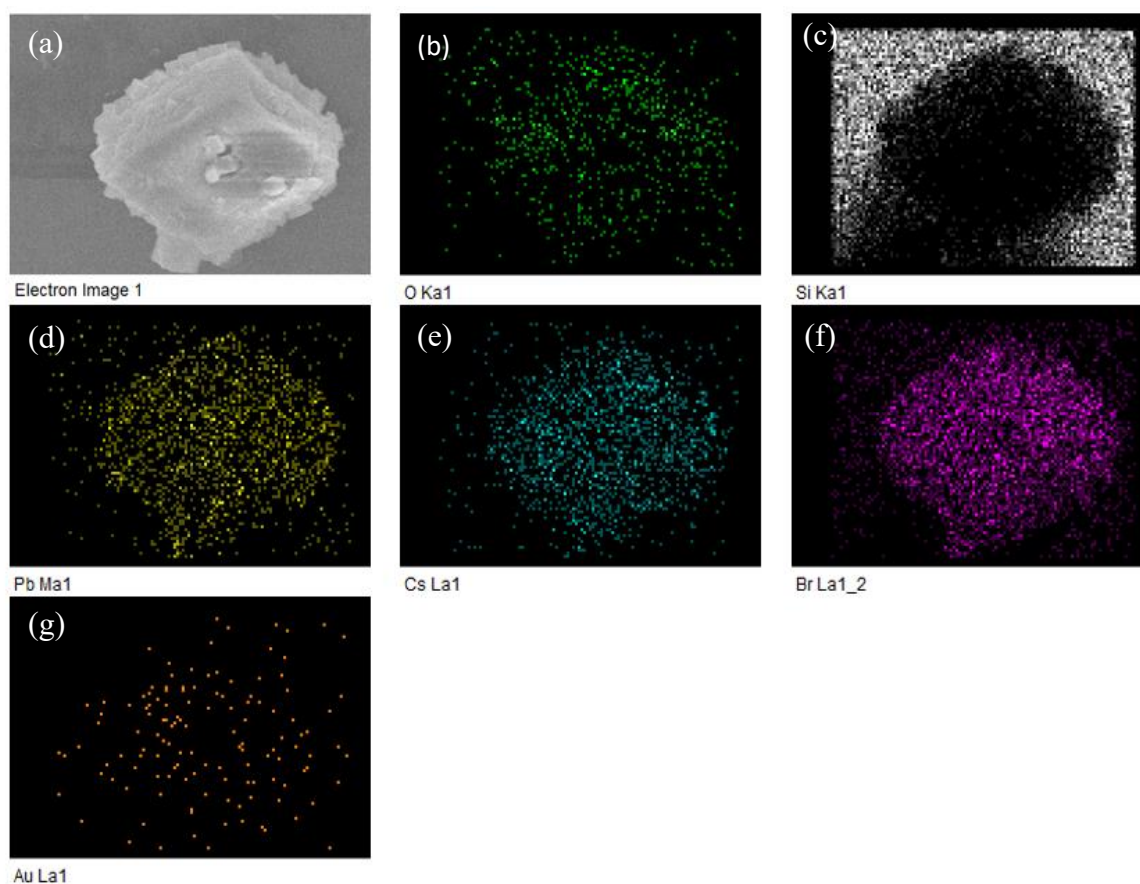
Figure 21: (a) Electronic structure of Au@SiO$_2$@CsPbBr$_3$. (b-f) Elemental color mapping of elements of Au@SiO$_2$@CsPbBr$_3$ by FESEM.

Thermogravimetric Analysis of $CsPbBr_3$ in comparison with $Au@SiO_2@CsPbBr_3$ shows that gold nanocomposite is more thermally stable than $CsPbBr_3$ by 26^oC, thus making it better to use in applications and solving the problem of thermal instability in $CsPbBr_3$.
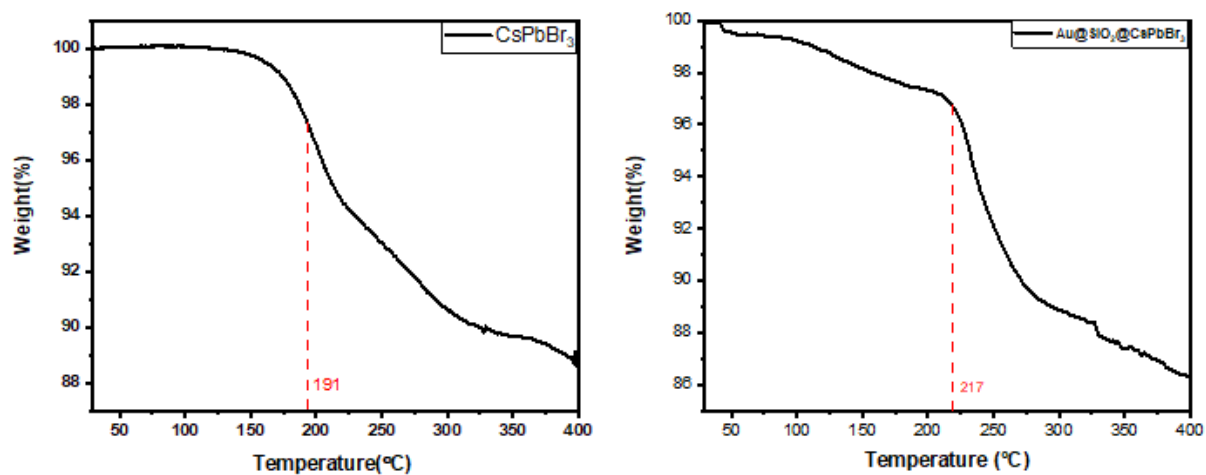
Figure 22: (a) TGA plot of CsPbBr3 (b) TGA plot of Au@SiO2@CsPbBr3.

CHAPTER 3

Synthesis and Characterization of Si nanocomposite (SiO$_2$@CsPbBr$_3$)

3.1 Experimental Section

3.1.1 Chemicals Required

Tetraethylorthosilicate (TEOS, C$_8$H$_{20}$O$_4$Si, >99%, Sigma-Aldrich), Sodium Hydroxide pellets (NaOH, 98%, Sisco Research Laboratories), Ammonium Hydroxide (NH$_4$OH), Lead (II) Bromide (PbBr$_2$, 98%, Sigma Aldrich), Cesium Bromide (CsBr, 99.9%, Alfa Aeser), N, N-Dimethylformamide(C$_3$H$_7$NO,99.8%, Sigma Aldrich), Ethanol(CH$_3$CH$_2$OH, Sigma Aldrich), Acetone(CH$_3$COCH$_3$, Sigma Aldrich), Ployvinylpyrrolidone(PVP, Sigma Aldrich), Ethylene glycol(C$_2$H$_6$O$_2$, 99.8%, Sigma Aldrich), Distilled Water, Hexane fraction from Petroleum (Merck Life Science Private Limited.

3.1.2 Synthesis of Monodisperse SiO$_2$ spheres (Radius less than 20nm)

In the 5 ml solution concentration of TEOS, distilled Water, NH$_4$OH, ethanol used are 0.17 M, 3 M, 0.11 M, and 5 M, respectively. Firstly, Ethanol, Distilled Water, and NH$_4$OH are added are stirred for 10 min. Following this, TEOS is added, and the solution is kept for ageing overnight. The solution was then centrifuged for 20 min at 13000 rpm to obtain a milkish-white precipitate. The precipitate is then dried at 60 ˚C.[40,41]

3.1.3 Impregnation of CsPbBr$_3$ on Monodisperse SiO$_2$ Spheres

The pellet is dissolved in a minimal amount of ethanol and is drop-casted on a clean glass slide (Washed with a soap-water solution and then given a quick boil in isopropanol). Then, 0.025 M PbBr$_2$ in N, N-Dimethylformamide is drop-casted and dried at 60 ˚C for 5 min. After that, 0.1 M

CsBr in ethanol-water (9:1) is drop-casted and dried at 60 ˚C for 2 min, and excess is wiped by Kimwipes. The slide is then kept under continuous vacuum for 1-2hr.

3.2 Results and Discussion

In order to grasp a good idea of the effect of plasmonic material, I thought of preparing a Silica nanocomposite and observe what impact does the absence of Au metal nanoparticle creates. For this, I had a vision of preparing a silica matrix with $CsPbBr_3$ inserted in it and compare both in terms of their decay rates and quantum yields. For this, monodisperse silica spheres of around 20 nm size are prepared using the popularly known "Stöber process". In this process, TEOS, NH_4OH, water and HCl are required. Here, hydrolysis of alkyl silicates and condensation of silicic acid takes place in alcoholic solutions using ammonia as a catalyst. On top of SiO_2 spheres, $CsPbBr_3$ is inserted like in the previous case with the intention that each silica sphere has $CsPbBr_3$ inside it. UV-Vis spectra of monodisperse Silica spheres confirmed their formation.
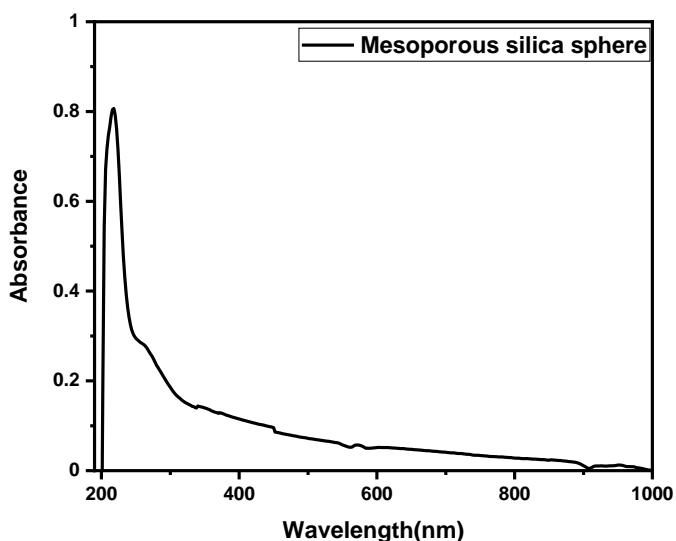
Figure 23: UV-Visible spectrum of monodisperse silica spheres.

Transmission Electron Microscopy images show the formation of monodisperse silica spheres of diameter less than 20 nm. The size mainly varied from 12-15 nm, which is appropriate for the comparison purpose with other nanocomposites.

25
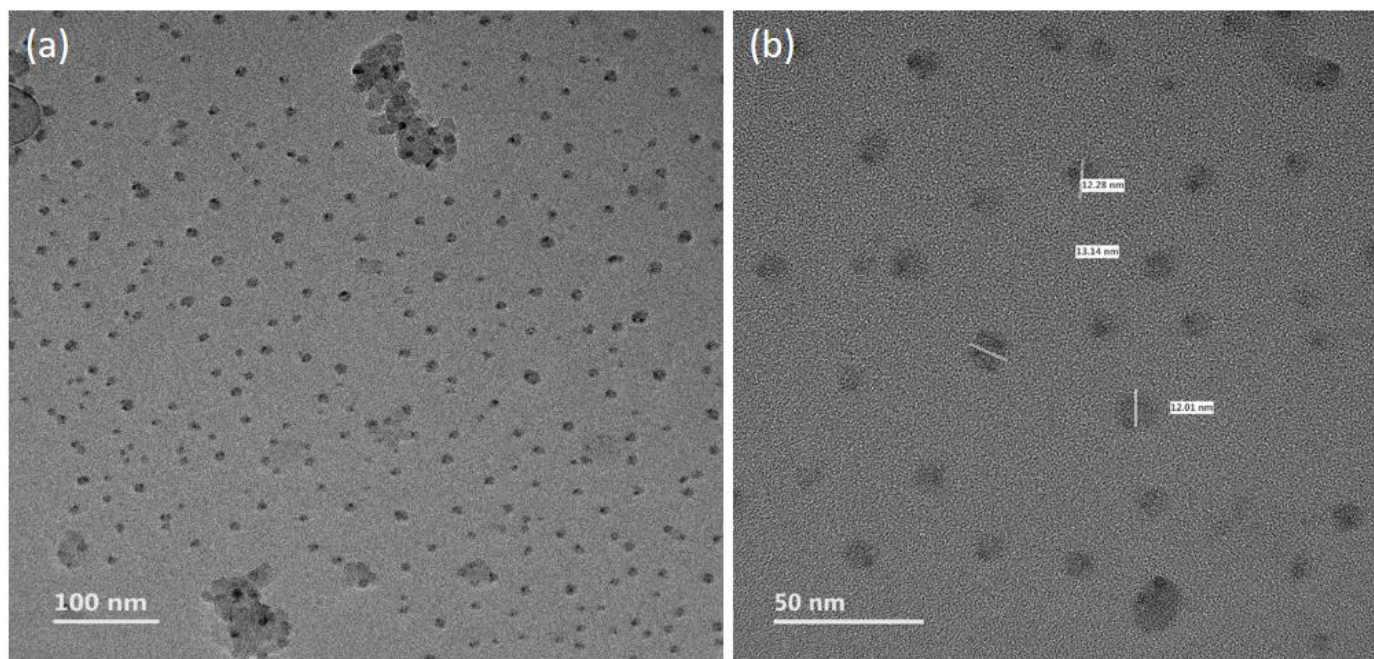
Figure 24: (a) TEM image of monodisperse silica spheres (b) TEM image depicting the diameter of monodisperse silica spheres (approximately 13 nm).

The TEM-EDX analysis (Energy Dispersive X-ray Spectra using Transmission Electron Spectroscopy) gives an insight into the chemical composition of SiO_2 spheres. Peaks corresponding to each constituent element is shown in the plot. The peak corresponding to non-constituent element C has been eliminated as it arises because of using the Carbon grid. The table below the graph gives information about the atomic % ratios present in SiO_2 spheres obtained from TEM-EDX analysis.
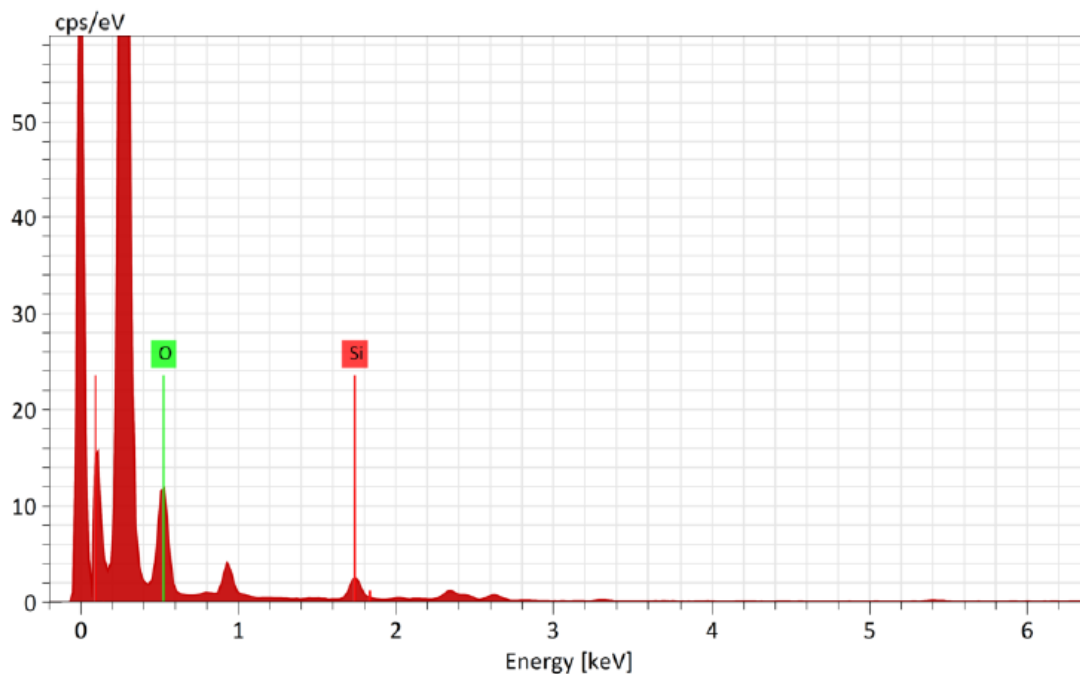
Figure 25: TEM-EDX analysis showing peaks of elements present in silica spheres.

Element	At. No.	Mass [%]	Atom [%]
Silicon	14	19.25	11.96
Oxygen	8	80.75	88.04
		100.00	100.00

Table 3: Atomic % ratio and mass % ratio of silica spheres.

Photoluminescence spectra of Silica spheres impregnated with $CsPbBr_3$ ($SiO_2@CsPbBr_3$) show the characteristic peak of $CsPbBr_3$ around 510 nm (here at 511 nm), confirming the presence of $CsPbBr_3$ in the nanospheres and the reason for luminescence in the nanocomposite formed.

When viewed under the excitation wavelength of 365 nm, a glass slide of $SiO_2@CsPbBr_3$ exhibits luminescence due to the presence of $CsPbBr_3$.
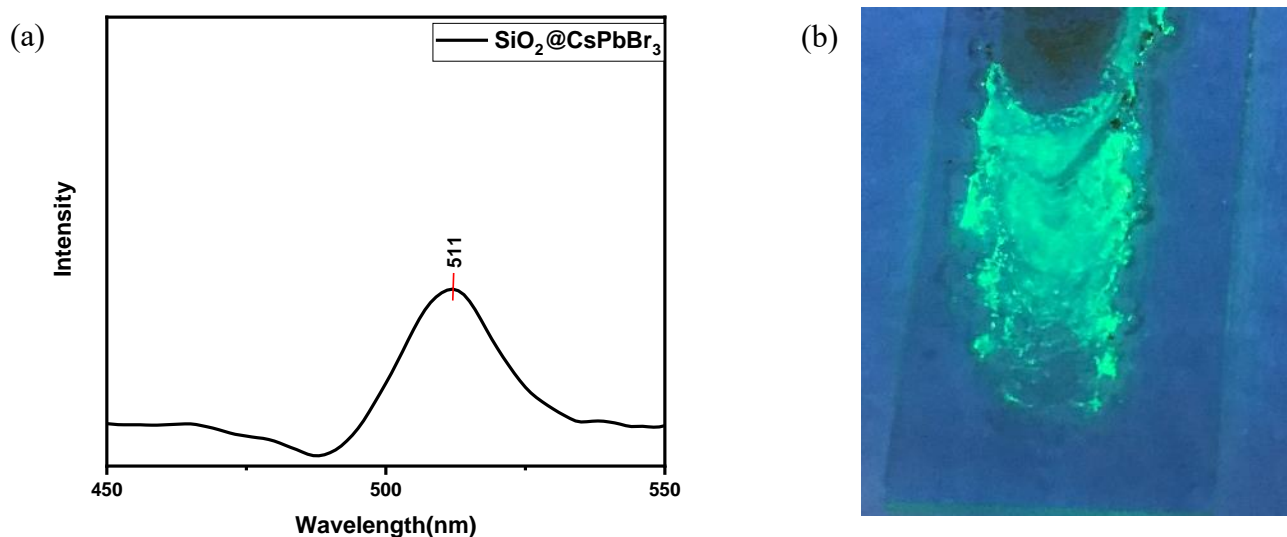
Figure 26: (a) PL spectra of $SiO_2@CsPbBr_3$ (b) $SiO_2@CsPbBr_3$ under UV light (λ_{exc} 365nm).

Elemental color mapping corresponding to each element is shown. It also confirms the presence of $CsPbBr_3$ in the nanocomposite.
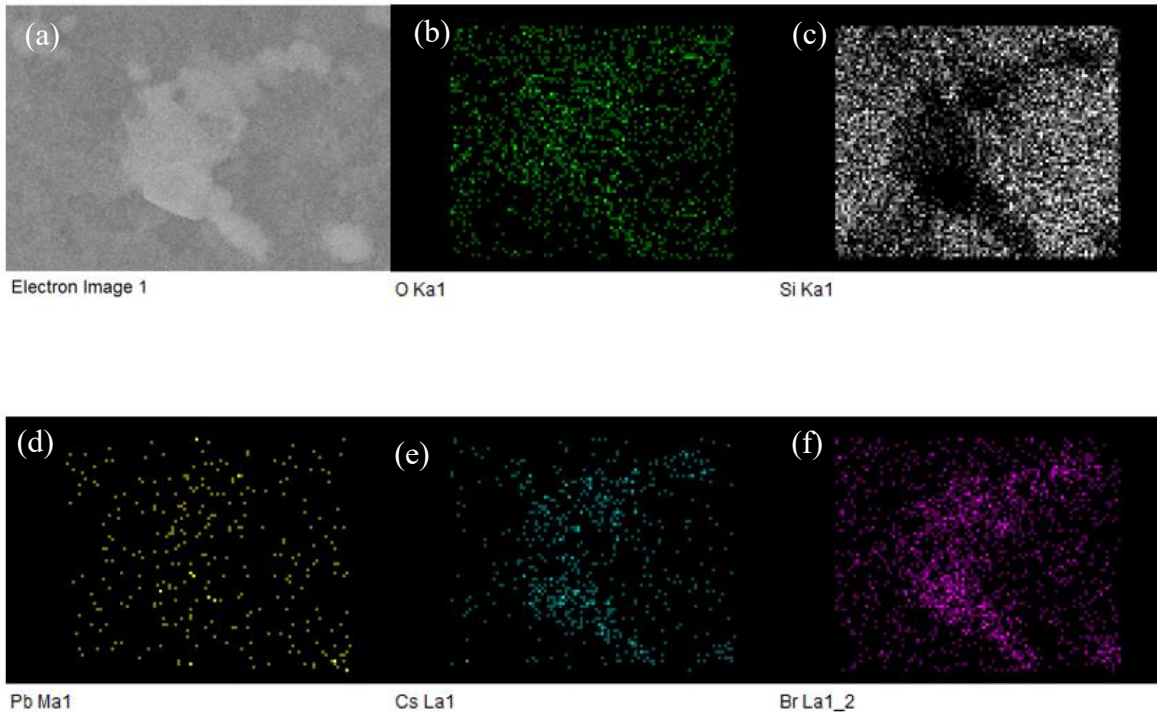
Figure 27: (a) Electronic structure of $SiO_2@CsPbBr_3$. (b-g) Elemental color mapping of elements of $Au@SiO_2@CsPbBr_3$ by FESEM.

Time-Correlated Single Photon Counting (TCSPC) gives the decay of $SiO_2@CsPbBr_3$ as 0.011ns.
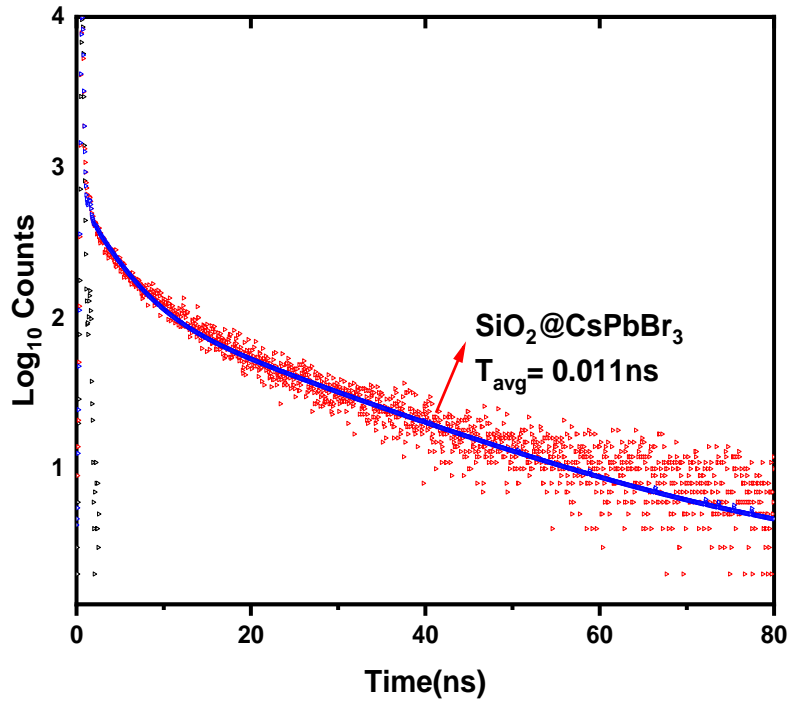
Figure 28: TCSPC of $SiO_2@CsPbBr_3$.

TRI-EXPONENTIAL FIT

Sample	A_1	A_2	A_3	T_1(ns)	T_2(ns)	T_3(ns)	T_{avg}(ns)	χ^2
SiO₂@CsPbBr₃	0.01	0.00	0.99	2.69	0.24	0.004	0.011	0.30

Table 4: Amplitude and corresponding lifetime of SiO_2@$CsPbBr_3$.

CHAPTER- 4

Synthesis and Characterization of Pd nanocomposite (Pd@SiO$_2$@CsPbBr$_3$)

4.1 Experimental Section

4.1.1 Chemicals Required

Potassium Bromide (KBr, 99%,Sigma Aldrich), Lead (II) Bromide (PbBr$_2$, 98%, Sigma Aldrich),Cesium Bromide (CsBr, 99.9%, Alfa Aeser), N,N-Dimethylformamide(C$_3$H$_7$NO,99.8%, Sigma Aldrich), Ethanol(CH$_3$CH$_2$OH, Sigma Aldrich), Acetone(CH$_3$COCH$_3$, Sigma Aldrich), Ployvinylpyrrolidone(PVP, Sigma Aldrich), Ethylene glycol(C$_2$H$_6$O$_2$, 99.8%, Sigma Aldrich),Hexane fraction from Petroleum (Merck Life Science Private Limited), and Palladium chloride (PdCl$_2$, 60%, LobaChemie).

4.1.2 Synthesis of Pd Nanorods

5 ml of Ethylene Glycol is put in 100 ml three-neck RB with a reflux condenser and Teflon-coated magnetic bead and heated at 100˚C. Two solutions are prepared simultaneously, one containing 46.6 mg of PdCl$_4$ $^{2-}$ and 60 mg of KBr dissolved in 3ml of water and the other containing 91.6 mg of PVP in 3ml of water. These solutions are injected simultaneously using two syringes in 2 min (drop by drop). The reaction mixture is heated at 100˚C for 1 hr. The product is then centrifuged and washed with acetone to form a precipitate and then with ethanol to remove excess Ethylene Glycol and PVP at 12000 rpm for 20 min.[42]
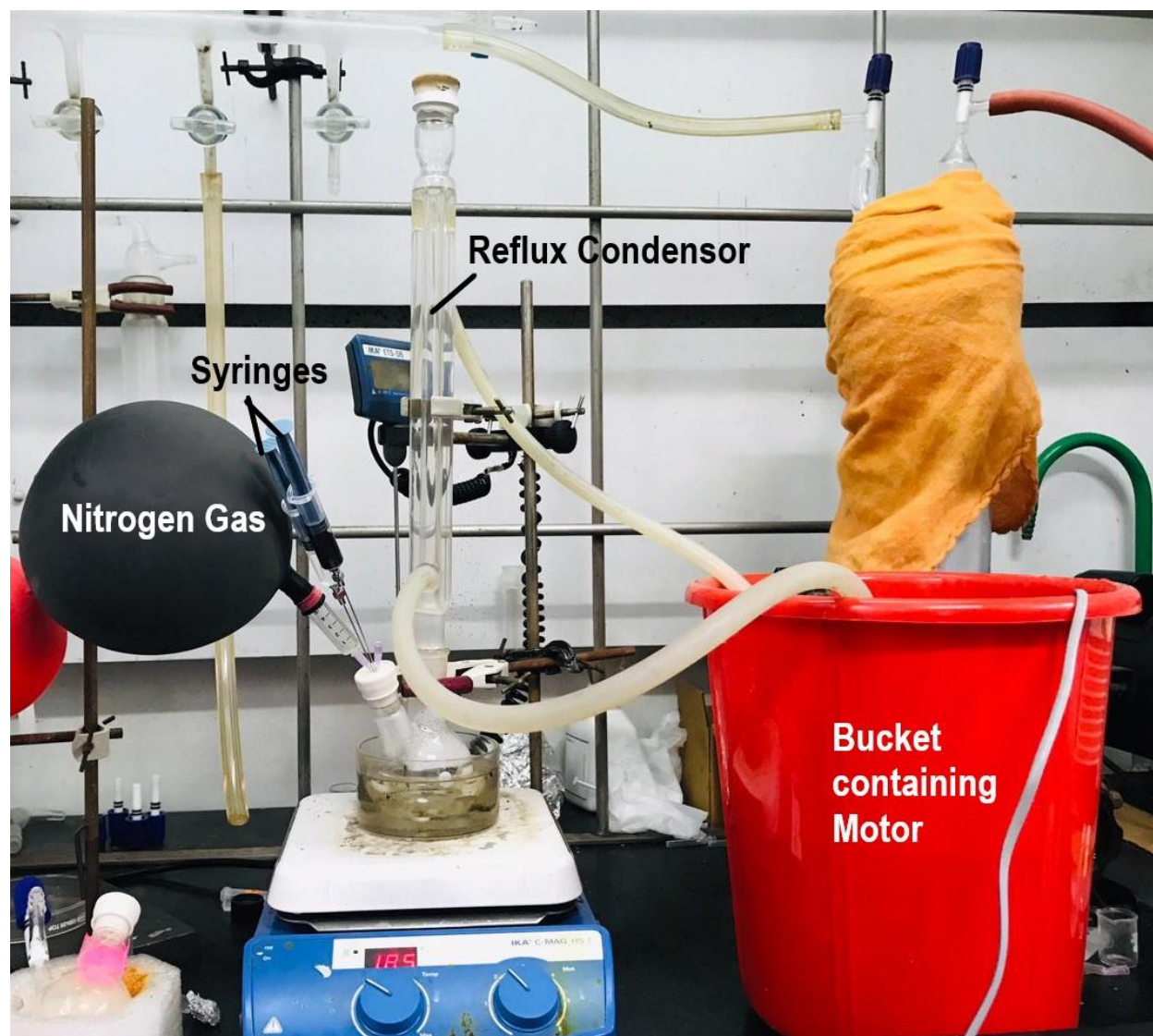
Figure 29: Experimental setup for the synthesis of Pd nanorods.

4.1.3 Synthesis of Silica Shell over Pd Nanorods

Silica shell is formed in the same way as described above.20 mM solution of CTAB is prepared, and 1ml of it is loaded to the solution. The solution is aged overnight. The solution is then kept at continuous stirring by adding 15 μl of 0.1 M of NaOH. After 30 min, 20 μl of 50 % TEOS in methanol is added. This addition is repeated twice after every 1 hr. The solution is then removed from stirring and kept for ageing for 24 hr. It is then washed with methanol for 30 min at 14000 rpm for 30 min to obtain a pellet.

4.1.4 Impregnation of CsPbBr$_3$ on Pd@SiO$_2$

Impregnation is also done in the same way as described above. The pellet is dissolved in a minimal amount of methanol and is drop-casted on a clean glass slide (Washed with a soap-water solution and then boiled in isopropanol). Then, 0.025 M PbBr$_2$ in N, N-Dimethylformamide is drop-casted and dried at 60 ˚C for 5 min. After that, 0.1M CsBr in ethanol-water (9:1) is drop-casted and dried at 60 ˚C for 2 min, and excess is wiped by Kim wipes. The slide is then kept under continuous vacuum for 1-2 hr. When it is completely dried, the powder is extracted and dissolved in hexane.

4.2 Results and Discussion

In order to check the impact of non-plasmonic material in comparison to a plasmonic material, we aimed to prepare a Pd nanocomposite which has Pd nanorods shelled with Silica and CsPbBr$_3$ inside the silica matrix. It is important to note that Pd metal nanoparticles are non-plasmonic only in visible range; however they do show plasmonic effects in UV and IR regions. Pd nanorods synthesis is done by using the famous polyol method. The bromide ion used in the synthesis procedure chemisorbs onto the surface of Pd seeds making changes in its facets.; PVP helps in the growth along with the nucleation process, and Ethylene Glycol helps in the reduction process.

Transmission Electron Microscopy (TEM) was used to confirm the formation of Pd nanorods. The Pd nanorods' aspect ratio ranges from 2 to 8. Pd nanorods UV-Visible spectrum indicate that there is no plasmonic frequency in the visible range, which is helpful for this analysis. At shorter wavelengths, however, it is plasmonic.
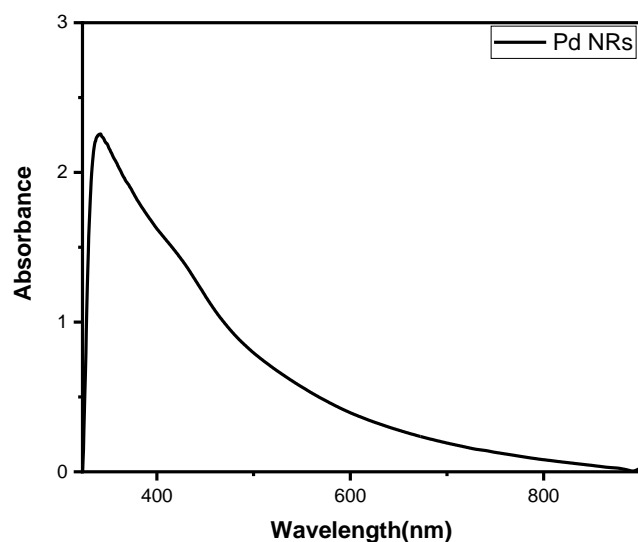
Figure 30: UV-Visible spectrum of Pd nanorods.

Pd nanorods are shelled with silica, and the formation of Pd@SiO$_2$ is also confirmed with the help of TEM. With a 24 hr ageing period, the shell thickness is about 10 nm.
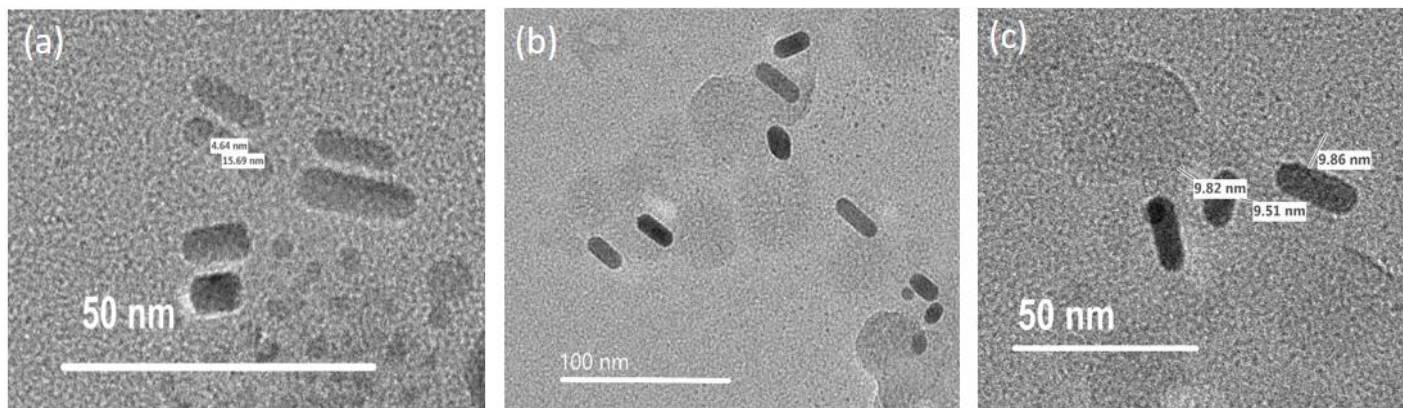
Figure 31: (a) TEM image of Pd Nanorods (b,c) TEM image of Pd@SiO$_2$.

Pd nanorod encapsulated inside mesoporous silica, has CsPbBr$_3$ in its pores. This is confirmed with the characteristic peak of CsPbBr$_3$ at 506 nm in the Photoluminiscence spectra. Glass slide of Pd@SiO$_2$@CsPbBr$_3$ shows luminiscence when seen under UV light (λ_{exc} 365 nm).
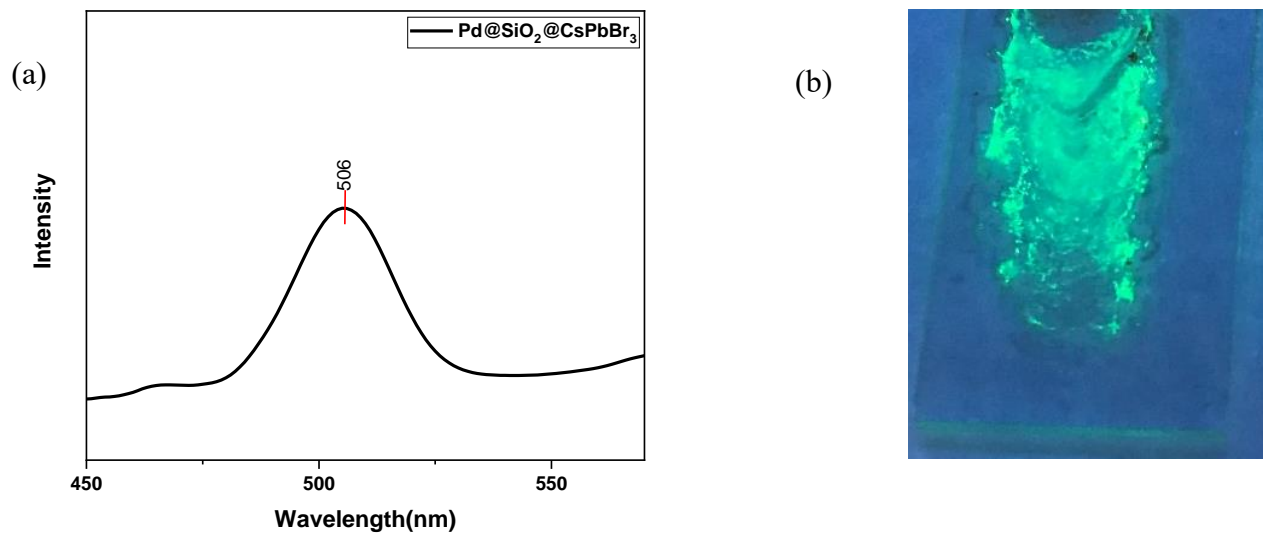
Figure 32: (a) PL spectra of Pd@SiO$_2$@CsPbBr$_3$ (b) Pd@SiO$_2$@CsPbBr$_3$ under UV light (λ_{exc} 365 nm).
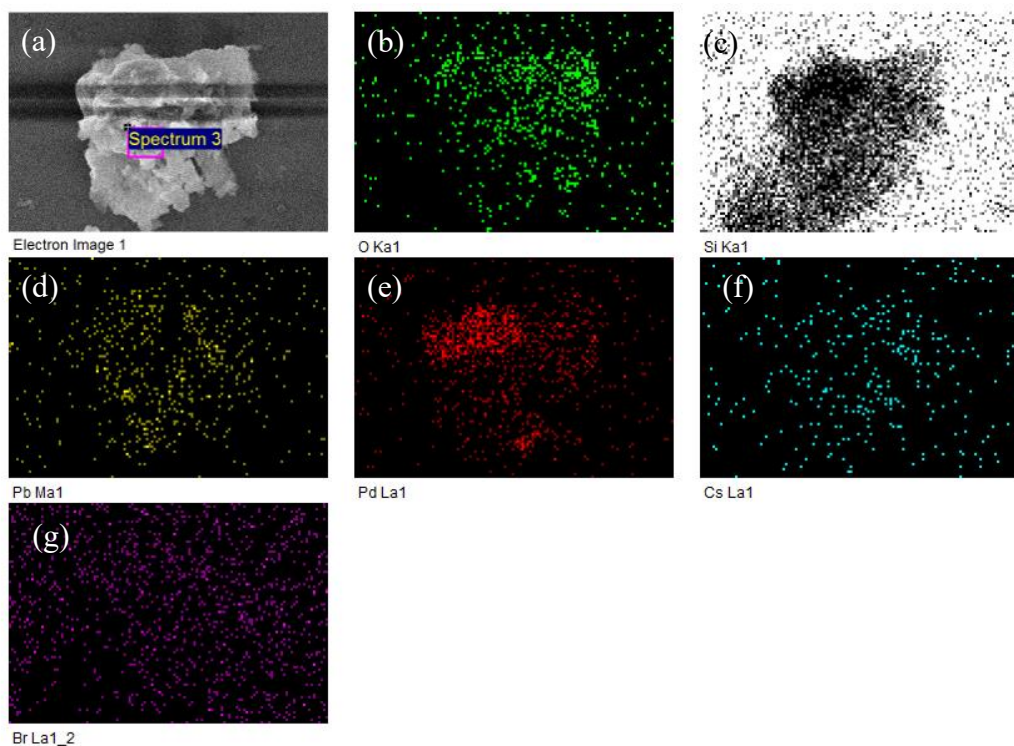
Figure 33 : (a) Electronic structure of SiO$_2$@CsPbBr$_3$. (b-g) Elemental color mapping of elements of Au@SiO$_2$@CsPbBr$_3$ by FESEM.
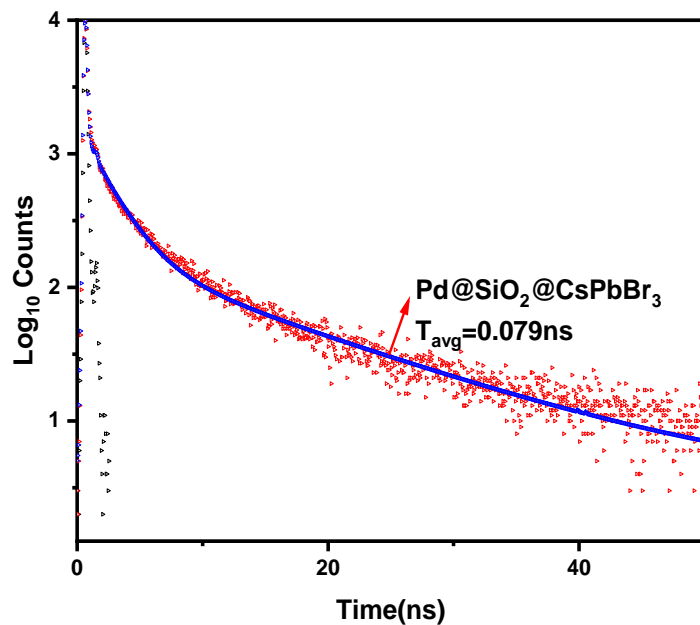
Figure 33: TCSPC of Pd@SiO_2@$CsPbBr_3$.

TRI-EXPONENTIAL FIT

Sample	A_1	A_2	A_3	T_1(ns)	T_2(ns)	T_3(ns)	T_{avg}(ns)	χ^2
Pd@SiO_2@$CsPbBr_3$	0.01	0.00	0.99	38.9	235	0.802	0.079	1.56

Table 5: Amplitude and corresponding lifetime of Pd@SiO_2@$CsPbBr_3$.

CHAPTER- 5

Comparison between nanocomposites and Application in LEDs

5.1 Lifetime Analysis

There is no periodic pattern in the lifetime decay of $CsPbBr_3$, $Au@SiO_2@CsPbBr_3$, $SiO_2@CsPbBr_3$ and $Pd@SiO_2@CsPbBr_3$. However, all the nanocomposites have decreased lifetime in comparison to $CsPbBr_3$. It was predicted that the lifetime would decline, increasing the quantum yield as the radiative decay increased. The influence of metal on radiative decay and nonradiative decay However, the decay times of $SiO_2@CsPbBr_3$ and $Pd@SiO_2@CsPbBr_3$ are 0.011 ns and 0.079 ns, respectively, which is suspicious. A considerable amount of decrement in lifetime of $Au@SiO_2@CsPbBr_3$ (3.59 ns) in comparison to $CsPbBr_3$ (6.57 ns) is potential for application in LEDs as decrement in lifetime means faster radiative decay which in turn leads to higher quantum yield.
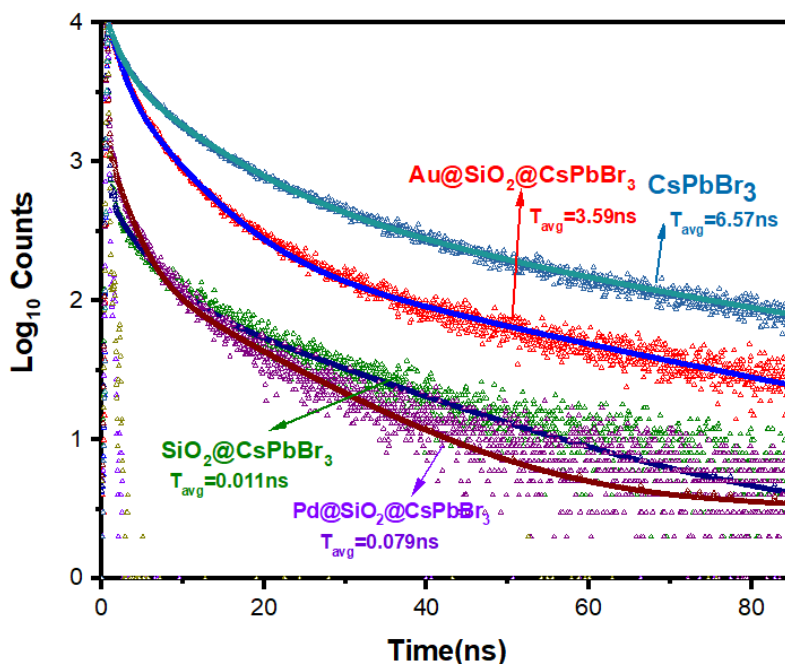
Figure 34: TCSPC of the three nanocomposites in comparison with $CsPbBr_3$.

TRI-EXPONENTIAL FIT

Sample	A_1	A_2	A_3	T_1(ns)	T_2(ns)	T_3(ns)	T_{avg}(ns)	χ^2
$CsPbBr_3$	0.37	0.08	0.55	8.15	32.51	1.70	6.57	1.23
$Au@SiO_2@CsPbBr_3$	0.34	0.10	0.56	3.80	21.0	0.42	3.59	1.67
$SiO_2@CsPbBr_3$	0.01	0.00	0.99	2.69	0.24	0.004	0.011	0.30
$Pd@SiO_2@CsPbBr_3$	0.01	0.00	0.99	38.9	235	0.802	0.079	1.56

Table 6: Amplitude and corresponding lifetime of $CsPbBr_3$ with the three nanocomposites.

5.2 Application in LEDs

5.2.1 Motivation

Mesoporous Silica acts as a protective layer for $CsPbBr_3$, as $CsPbBr_3$ is readily exposed to oxygen and moisture on its own. $CsPbBr_3$ mixed with $CsPb(Br_{0.4} I_{0.6})_3$ in silica resin has been found useful for LEDs.[43] Anion exchange method has been always followed to tune wavelengths, However, for LED packaging it should be avoided. Gold nanoparticles alone with emissive layer outside were also found useful in LEDs. [44] Thus, taking inspiration from both the works, In our case mesoporous Silica will prevent anion exchange acting as a protective shell, and Au nanorods will satisfy the need of characteristic wavelength required. We can also use polymer PEDOT:PSS as hole injection layer and polumer TFB as a hole transport layer or any other combination of electron and hole transport layer to use it in applications.

5.2.2 Problem

The nanocomposite Au@SiO_2@ $CsPbBr_3$ as well as both the other nanocomposites were prepared on a glass slide. The nanocomposites were not fully soluble when I tried to extract the powder and disperse it in the appropriate solvents. The powder would settle instantaneously and it was difficult to record spectra.

5.2.3 Solvents Used

The list of solvents used are as follows-

- Hexane
- Toulene
- Tetrahydrofuran
- Dichloromethane
- Diethylether
- Isopropanol
- Acetone
- Dimethylformamide,
- Acetonitrile
- Varying proportions of Diethylchloromethane and Diethylether
- Varying proportions of Tetrahydrofuran and Diethylether.

    Out of these, Acetone was the one that dispersed it the best and also exhibited luminescence.

    We attempted to spin coat a layer of Au@ SiO_2@ $CsPbBr_3$ on top of TiO_2 as it is an electron transport layer to see if the coating could be uniform and pave its way to LED applications.

5.2.4 Procedure

The TiO_2 layer was created by adding 0.6 -0.8 mL of titanium(IV) isopropoxide in 6-6.5 mL of ethanol while stirring. It was then followed by subsequent addition of 0.125 mL of HCl (37 weight percent, ACS grade, Merck). The reaction mixture was stirred continuously for an additional hour, and the resulting sol was used to create the TiO_2 film on the silicon wafer (Cleaned with 10% Hydrofluoric acid solution) with the help of a spin-coating machine at 3000

rotations per minute. The rutile form of TiO$_2$ film was ready for use in the following step after drying at 60 °C in a hot air oven and then calcination at 450 °C, preferably in a muffle furnace. Au@SiO$_2$@ CsPbBr$_3$ was then dispersed in acetone and spin-coated on the same wafer at 2500 rotations per minute. The SEM wafer was then kept under continuous vacuum for 1 hr.[45]
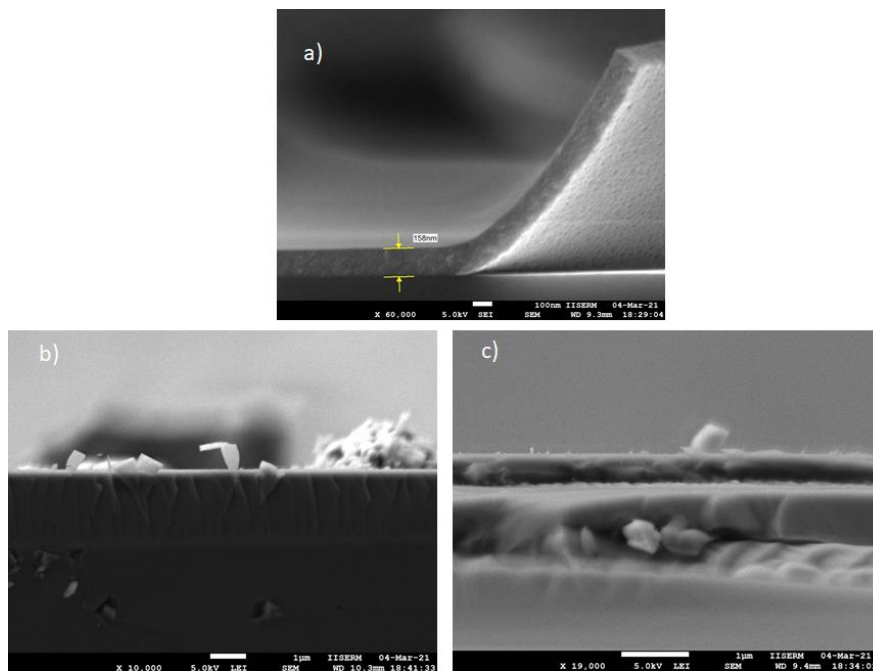
Figure 35: (a) FESEM image of TiO$_2$ layer (b) FESEM image of Au@ SiO$_2$@ CsPbBr$_3$

Conclusion

Au@SiO$_2$@CsPbBr$_3$, SiO$_2$@CsPbBr$_3$ and Pd@SiO$_2$@CsPbBr$_3$ nanocomposites have been successfully synthesized and characterized. In the lifetimes of CsPbBr$_3$, Au@SiO$_2$@CsPbBr$_3$, SiO$_2$@CsPbBr$_3$, and Pd@SiO$_2$@CsPbBr$_3$, there is no evidence of an expected periodic trend. Decay times of SiO$_2$@CsPbBr$_3$ and Pd@SiO$_2$@CsPbBr$_3$ are 0.011ns and 0.079ns, respectively, which are suspicious and require more study. A considerable amount of decrement in lifetime of Au@SiO$_2$@CsPbBr$_3$ (3.59ns) in comparison to CsPbBr$_3$ (6.57ns) is potential for application in LEDs. The thermal stability and higher photoluminescence intensity of Au@SiO$_2$@CsPbBr$_3$ are higher in comparison to CsPbBr$_3$, thus adding to its merit for LEDs. Thus, the gold nanocomposite is of utmost importance for exploring applications in LEDs. Non-Plasmonic material didn't show much difference when added, signifying the importance of plasmonic materials over them.

Future Outlook

The work presented in this thesis emphasizes the importance of plasmonic material mainly Au in the vicinity of CsPbBr$_3$ as the fluorophore. The study is useful as it enlists the synthesizes and comparison by various characterization techniques of similar kind nanocomposites. The useful increment in quantum yield and thermal stability of Au nanocomposite is helpful for application in LEDs. We would like to do the electroluminescence study of Au nanocomposite to confirm its application in LEDs.

Bibliography

1. Chouhan, L.; Ghimire, S.; Subrahmanyam, C.; Miyasaka, T.; Biju, V. Synthesis, Optoelectronic Properties and Applications of Halide Perovskites. *Chem. Soc. Rev.* **2020**, *49*, 2869–2885.

2. Travis, W.; Glover, E. N. K.; Bronstein, H.; Scanlon, D. O.; Palgrave, R. G. On the Application of the Tolerance Factor to Inorganic and Hybrid Halide Perovskites: A Revised System. *Chem. Sci.* **2016**, *7*, 4548–4556.

3. Yun, J. H.; Polyakov, A. Y.; Kim, K. C.; Yu, Y. T.; Lee, D.; Lee, I. H. Enhanced Luminescence of $CsPbBr_3$ Perovskite Nanocrystals on Stretchable Templates with Au/SiO_2 Plasmonic Nanoparticles. *Optics letters* **2018**, *43*, 2352–2355.

4. Knoblauch, R.; Hamo, H. B.; Marks, R.; Geddes, C. D. Spectral Distortions in Zinc-Based Metal-Enhanced Fluorescence Underpinned by Fast and Slow Electronic Transitions. *Chem. Phys. Lett.* **2020**, *744*, 137212.

5. Unser, S.; Bruzas, I.; He, J.; Sagle, L. Localized Surface Plasmon Resonance Biosensing: Current Challenges and Approaches. *Sensors (Basel)* **2015**, *15*, 15684–15716.

6. Vieira, G. M.; B., M.; S., N.; Barros, E. B.; Reich, S. Plasmonic Properties of Close-Packed Metallic Nanoparticle Mono-and Bilayers. *The Journal of Physical Chemistry C* **2019**, *123*, 17951–17960.

7. Wang, L.; Hasanzadeh Kafshgari, M.; Meunier, M. Optical Properties and Applications of Plasmonic-Metal Nanoparticles. *Advanced Functional Materials* **2020**, *30*, 2005400.

8. Fothergill, S. M.; Joyce, C.; Xie, F. Metal Enhanced Fluorescence Biosensing: From Ultra-Violet towards Second near-Infrared Window. *Nanoscale* **2018**, *10*, 20914–20929.

9. Yi, Z.; Ladi, N. H.; Shai, X.; Li, H.; Shen, Y.; Wang, M. Will Organic–Inorganic Hybrid Halide Lead Perovskites Be Eliminated from Optoelectronic Applications? *Nanoscale adv.* **2019**, *1*, 1276–1289.

10. Goetz, K. P.; Taylor, A. D.; Paulus, F.; Vaynzof, Y. Shining Light on the Photoluminescence Properties of Metal Halide Perovskites. *Adv. Funct. Mater.* **2020**, *30*, 1910004.

11. Samanta, A.; Zhou, Y.; Zou, S.; Yan, H.; Liu, Y. Fluorescence Quenching of Quantum Dots by Gold Nanoparticles: A Potential Long Range Spectroscopic Ruler. *Nano Lett.* **2014**, *14*, 5052–5057.

12. Pillai, S.; Beck, F. J.; Catchpole, K. R.; Ouyang, Z.; Green, M. A. The Effect of Dielectric Spacer Thickness on Surface Plasmon Enhanced Solar Cells for Front and Rear Side Depositions. *J. Appl. Phys.* **2011**, *109*, 073105.

13. Yang, J.; Liu, Z.; Hu, Z.; Zeng, F.; Zhang, Z.; Yao, Y.; Yao, Z.; Tang, X.; Du, J.; Zang, Z.; Pi, M.; Liu, L.; Leng, Y. Enhanced Single-Mode Lasers of All-Inorganic Perovskite Nanocube by Localized Surface Plasmonic Effect from Au Nanoparticles. *J. Lumin.* **2019**, *208*, 402–407.

14. Zhang, Y.; Sun, H.; Zhang, S.; Li, S.; Wang, X.; Zhang, X.; Liu, T.; Guo, Z. Enhancing Luminescence in All-Inorganic Perovskite Surface Plasmon Light-Emitting Diode by Incorporating Au-Ag Alloy Nanoparticle. *Opt. Mater. (Amst.)* **2019**, *89*, 563–567.

15. Pan, J.; Chen, J.; Zhao, D.; Huang, Q.; Khan, Q.; Liu, X.; Tao, Z.; Zhang, Z.; Lei, W. Surface Plasmon-Enhanced Quantum Dot Light-Emitting Diodes by Incorporating Gold Nanoparticles. *Opt. Express* **2016**, *24*, A33-43.

16. Xia, Z.; Zhang, C.; Feng, Z.; Wu, Z.; Wang, Z.; Chen, X.; Huang, S. Synergetic Effect of Plasmonic Gold Nanorods and MgO for Perovskite Solar Cells. *Nanomaterials (Basel)* **2020**, *10*, 1830-1835.

17. Balakrishnan, S. K.; Kamat, P. V. Au–CsPbBr3 Hybrid Architecture: Anchoring Gold Nanoparticles on Cubic Perovskite Nanocrystals. *ACS Energy Lett.* **2017**, *2*, 88–93.

18. Zhang, X.; Xu, B.; Wang, W.; Liu, S.; Zheng, Y.; Chen, S.; Wang, K.; Sun, X. W. Plasmonic Perovskite Light-Emitting Diodes Based on the Ag–CsPbBr$_3$ System. *ACS Appl. Mater. Interfaces* **2017**, *9*, 4926–4931

19. Yun, J. H.; Polyakov, A. Y.; Kim, K. C.; Yu, Y. T.; Lee, D.; Lee, I. H. Enhanced Luminescence of CsPbBr$_3$ Perovskite Nanocrystals on Stretchable Templates with Au/SiO$_2$ Plasmonic Nanoparticles. *Optics letters* **2018**, *43*, 2352–2355.

20. Dadı, S.; Altıntas, Y.; Beskazak, E.; Mutlugun, E. Plasmon Enhanced Emission of Perovskite Quantum Dot Films. *MRS Adv.* **2018**, *3*, 733–739.

21. Fan, R.; Wang, L.; Chen, Y.; Zheng, G.; Li, L.; Li, Z.; Zhou, H. Tailored Au@ TiO$_2$ Nanostructures for the Plasmonic Effect in Planar Perovskite Solar Cells. *Journal of Materials Chemistry A* **2017**, *5*, 12034–12042.

22. Mali, S. S.; Shim, C. S.; Kim, H.; Patil, P. S.; Hong, C. K. In Situ Processed Gold Nanoparticle-Embedded TiO$_2$ Nanofibers Enabling Plasmonic Perovskite Solar Cells to Exceed 14% Conversion Efficiency. *Nanoscale* **2016**, *8*, 2664–2677.

23. West, P. R.; Ishii, S.; Naik, G. V.; Emani, N. K.; Shalaev, V. M.; Boltasseva, A. Searching for Better Plasmonic Materials. *Laser Photon. Rev.* **2010**, *4*, 795–808.

24. Maiti, S.; Ghosh, M.; Das, P. K. Gold Nanorod in Reverse Micelles: A Fitting Fusion to Catapult Lipase Activity. *Chem. Commun. (Camb.)* **2011**, *47*, 9864–9866.

25. Park, K.; Biswas, S.; Kanel, S.; Nepal, D.; Vaia, R. A. Engineering the Optical Properties of Gold Nanorods: Independent Tuning of Surface Plasmon Energy, Extinction Coefficient, and Scattering Cross Section. *J. Phys. Chem. C Nanomater. Interfaces* **2014**, *118*, 5918–5926.

26. Truong, P. L.; Kim, B. W.; Sim, S. J. Rational Aspect Ratio and Suitable Antibody Coverage of Gold Nanorod for Ultra-Sensitive Detection of a Cancer Biomarker. *Lab Chip* **2012**, *12*, 1102–1109.

27. Rong, Y.; Dandapat, A.; Huang, Y.; Sasson, Y.; Zhang, L.; Dai, L.; Zhang, J.; Guo, Z.; Chen, T. Spatially-Controlled Growth of Platinum on Gold Nanorods with Tailoring Plasmonic and Catalytic Properties. *RSC Adv.* **2016**, *6*, 10713–10718.

28. Tian, L.; Chen, E.; Gandra, N.; Abbas, A.; Singamaneni, S. Gold Nanorods as Plasmonic Nanotransducers: Distance-Dependent Refractive Index Sensitivity. *Langmuir* **2012**, *28*, 17435–17442.

29. Shi, Y. Z.; Xiong, S.; Chin, L. K.; Zhang, J. B.; Ser, W.; Wu, J. H.; Chen, T. N.; Yang, Z. C.; Hao, Y. L.; Liu, A. Q. Determination of Size and Refractive Index of Single Gold Nanoparticles Using an Optofluidic Chip. *AIP Adv.* **2017**, *7*, 095024.

30. Asefa, T.; Tao, Z. Biocompatibility of Mesoporous Silica Nanoparticles. *Chem. Res. Toxicol.* **2012**, *25*, 2265–2284.

31. Kim, D.; Zuidema, J. M.; Kang, J.; Pan, Y.; Wu, L.; Warther, D.; Arkles, B.; Sailor, M. J. Facile Surface Modification of Hydroxylated Silicon Nanostructures Using Heterocyclic Silanes. *J. Am. Chem. Soc.* **2016**, *138*, 15106–15109.

32. Wu, L.; Jiao, Z.; Wu, M.; Song, T.; Zhang, H. Formation of Mesoporous Silica Nanoparticles with Tunable Pore Structure as Promising Nanoreactor and Drug Delivery Vehicle. *RSC Adv.* **2016**, *6*, 13303–13311.

33. Wu, W.-C.; Tracy, J. B. Large-Scale Silica Overcoating of Gold Nanorods with Tunable Shell Thicknesses. *Chem. Mater.* **2015**, *27*, 2888–2894.

34. Wrigglesworth, E. G.; Johnston, J. H. The Use of Dual Reductants in Gold Nanoparticle Syntheses. *RSC Adv.* **2017**, *7*, 45757–45762.

35. Nayak, D. R.; Bhat, N.; Venkatapathi, M.; Umapathy, S. Impact of Ultrathin Dielectric Spacers on SERS: Energy Transfer between Polarized Charges and Plasmons. *J. Mater. Chem. C Mater. Opt. Electron. Devices* **2017**, *5*, 2123–2129.

36. Gorelikov, I.; Matsuura, N. Single-Step Coating of Mesoporous Silica on Cetyltrimethyl Ammonium Bromide-Capped Nanoparticles. *Nano Lett.* **2008**, *8*, 369–373.

37. Orendorff, C. J.; Murphy, C. J. Quantitation of Metal Content in the Silver-Assisted Growth of Gold Nanorods. *J. Phys. Chem. B* **2006**, *110*, 3990–3994.

38. Fang, L.; Wang, W.; Liu, Y.; Xie, Z.; Chen, L. Janus Nanostructures Formed by Mesoporous Silica Coating Au Nanorods for Near-Infrared Chemo-Photothermal Therapy. *J. Mater. Chem. B Mater. Biol. Med.* **2017**, *5*, 8833–8838.

39. Kobayashi, Y.; Inose, H.; Nakagawa, T.; Gonda, K.; Takeda, M.; Ohuchi, N.; Kasuya, A. Control of Shell Thickness in Silica-Coating of Au Nanoparticles and Their X-Ray Imaging Properties. *J. Colloid Interface Sci.* **2011**, *358*, 329–333.

40. Greasley, S. L.; Page, S. J.; Sirovica, S.; Chen, S.; Martin, R. A.; Riveiro, A.; Hanna, J. V.; Porter, A. E.; Jones, J. R. Controlling Particle Size in the Stöber Process and Incorporation of Calcium. *J. Colloid Interface Sci.* **2016**, *469*, 213–223.

41. Sharma, J.; Polizos, G. Hollow Silica Particles: Recent Progress and Future Perspectives. *Nanomaterials (Basel)* **2020**, *10*, 1599.

42. Xiong, Y.; Cai, H.; Wiley, B. J.; Wang, J.; Kim, M. J.; Xia, Y. Synthesis and Mechanistic Study of Palladium Nanobars and Nanorods. *J. Am. Chem. Soc.* **2007**, *129* , 3665–3675.

43. Song, Y. H.; Choi, S. H.; Yoo, J. S.; Kang, B. K.; Ji, E. K.; Jung, H. S.; Yoon, D. H. Design of Long-Term Stable Red-Emitting CsPb(Br$_{0.4}$, $_{I0. 6}$)$_3$ Perovskite Quantum Dot Film for Generation of Warm White Light. *Chem. Eng. J.* **2017**, *313*, 461–465.

44. Park, J. H.; Lim, Y. T.; Park, O. O.; Kim, J. K.; Yu, J.-W.; Kim, Y. C. Polymer/Gold Nanoparticle Nanocomposite Light-Emitting Diodes: Enhancement of Electroluminescence Stability and Quantum Efficiency of Blue-Light-Emitting Polymers. *Chem. Mater.* **2004**, *16*, 688–692.

45. Mishra, S.; Takhellambam, D.; De, A. K.; Jana, D. Stable CsPbI3-Mesoporous Alumina Composite Thin Film at Ambient Condition: Preparation, Characterization, and Study of Ultrafast Charge-Transfer Dynamics. *J. Phys. Chem. C Nanomater. Interfaces* **2021**, *125*, 3285–3294.